LINE-OF-SIGHT PROPAGATION PHENOMENA

by

A. D. Wheelon and R. B. Muchmore

DISCLAIMER NOTICE

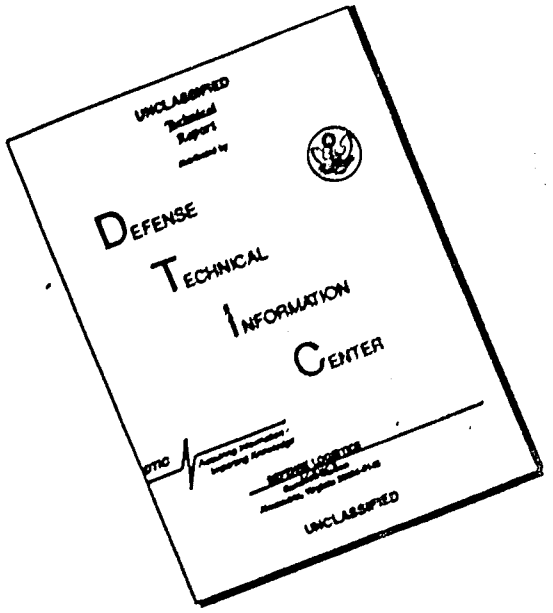

THIS DOCUMENT IS BEST QUALITY AVAILABLE. THE COPY FURNISHED TO DTIC CONTAINED A SIGNIFICANT NUMBER OF PAGES WHICH DO NOT REPRODUCE LEGIBLY.

LINE-OF-SIGHT PROPAGATION PHENOMENA

by

Albert D. Wheelon

and

R. B. Muchmore

Research Laboratory

The Ramo-Wooldridge Corporation
Los Angeles 45, California

SUMMARY

Turbulent and precipitation conditions in the real atmosphere are considered in their effect on the line-of-sight propagation of electromagnetic waves. It is found that tropospheric scattering and phase scintillation mechanisms place an interesting limit on the accuracy with which one may determine the angular position of a distant radiator. Superposition of the same perturbed signals gives rise to waveform distortion in communication systems. Theoretical expressions for angular power distributions and phase error spectra are derived from phenomenological atmospheric models. Ray bending by cloud formations and rainstorms is also computed for representative weather conditions.

I. INTRODUCTION

The present report summarizes the results of an investigation initiated to answer the simple question: "With what precision can one propagate microwave electromagnetic energy along a line-of-sight path in the real atmosphere?" Such a question arises naturally if one asks for the ultimate accuracy of radio location measurements or ultra-high speed communication techniques. One can imagine a variety of scattering and phase shifting mechanisms which might operate in the atmosphere to produce angle of arrival problems, multipath propagation modes, signal phase scintillation, and broadening of received energy patterns.

This study was fortunate in that considerable attention has recently been focused on the atmosphere in connection with beyond-line-of-sight (scatter) communication systems. A theory of turbulence scattering has been proposed[1],[2] to account for observed propagation anomolies. There has subsequently been initiated a thoroughgoing examination of the atmosphere and its variations. In addition to the usual meteorological disturbances (snow, rain, clouds, and dust), an atmospheric fine structure extending from the very surface of the earth to ionospheric heights has thereby been uncovered. This structure is measured as time and space varying concentrations of index of refraction in the troposphere and free electron densities in the ionosphere.

---

[1] H. G. Booker and W. E. Gordon, Proc. I.R.E., 41, 284 (1950).
[2] C. L. Pekeris, Proc. I.R.E., 35, 453 (1947).

The present study has exploited phenomenological models for turbulence and precipitation scattering which have been fitted to such experiments. Effects of clouds and elevated layers are computed from estimated departures of the index of refraction from its median values. In general, no attempt has been made to determine the effects of signal attenuation, * ducting or uniform horizontal layers. The essential output of the following calculation is: (1) RMS phase error and scintillation spectra for single rays and for linear superposition of multipath signals, and (2) angle of arrival variations for single rays and angular distributions for the scattered energy. No account is taken in this report of the stratified nature of the atmosphere; only deviations from the mean are considered. These results are computed for one receiving antenna only, so that in order to predict performance limits, one must employ the characteristics of the particular system contemplated. This study indicates two points rather clearly: (1) the atmosphere can be a limiting factor in very accurate radio location schemes, and (2) attendent phase variations imply a real distortion limit for ultra-high speed communication systems.

II. TROPOSPHERIC TURBULENCE

The troposphere is in continuous turbulent motion, and is therefore neither uniformly stratified nor homogeneously mixed. At a given instant there are both horizontal and vertical fluctuations in the temperature, pressure, and humidity about their respective means. One may think of

*Except insofar as this is necessary to secure convergence (and thus proper physical description) for wide-angle acceptance receiving antennae.

these micrometeorological disturbances as a turbulent boundary layer phenomenon associated with motion of the winds over the earth's rough surface. A detailed eddy decay scheme has been suggested which imagines these large scale wind-produced turbulence clusters to subdivide until their size and energy are eventually absorbed in molecular friction.[3],[4] We shall base our development on a purely phenomenological description of these tropospheric variations. The statistical properties of the troposphere's dielectric constant, and hence its index of refraction, are given by the normalized space correlation function

$$\rho(\vec{r}_{12}) = \frac{\langle \Delta\epsilon^*(r_1)\, \Delta\epsilon(r_2) \rangle}{\left\langle \left| \Delta\epsilon(r) \right|^2 \right\rangle} \qquad (2.1)$$

where $\vec{r}_{12}$ is the vector distance between points (1) and (2). $\Delta\epsilon$ is the variation of the dielectric constant about its mean. This function defines the (normalized) cross correlation between simultaneous records of dielectric constant taken at two points a distance r apart. The atmosphere is assumed to be isotropic and homogeneous, so that $\rho(\vec{r})$ is a function neither of the direction nor the end points of $\vec{r}$.

Limited tests[5],[6] tend to support the exponential correlation

---

[3] F. Villars and V. F. Weisskopf, Phys. Rev., 94, 232 (1954). They have given a fuller theory of turbulence scattering based on the Navier-Stokes equation. Their paper also contains references to the previous work of Heisenberg, Batchelor, and others.

[4] P. B. MacCready, Jr., Jour. of Meteor., 10, 434 (1953).

[5] J. R. Gerhardt, C. M. Crain, and H. W. Smith, Jour. of Meteorology, 9, 299 (1952).

[6] G. Birnbaum, Phys. Rev., 82, 110 (1951).

$$\rho(\vec{r}_{12}) = e^{-\frac{|r_{12}|}{\ell_o}} \tag{2.2}$$

where ℓ_o is a measure of the scale of the turbulence.

Detailed measurements have shown that the isotropic assumption is not strictly true; the scale length ℓ_o differs in horizontal and vertical directions, at least near the ground. Direct measurement[7] has also shown that this scale increases somewhat with altitude. Variations in the measurements of scale length with location[7] and time of day are so large that it was not considered worthwhile to use anything more sophisticated than Equation (2.2)[8].

Using Eq. (2.2), Booker and Gordon[1] have shown that the power scattered per unit solid angle, per unit incident power density, and per unit volume is given by

$$\sigma(\theta, \chi) = \frac{\left\langle \left| \frac{\Delta e}{e} \right|^2 \right\rangle \left(\frac{2\pi \ell_o}{\lambda}\right)^3 \sin^2(\chi)}{\lambda \left[1 + \left(\frac{4\pi \ell_o}{\lambda}\right)^2 \sin^2\left(\frac{\theta}{2}\right)\right]^2} . \tag{2.3}$$

λ denotes the wavelength of the incident radiation and χ is the angle between the incident electric field vector and the direction of scattering. θ is the angle included between the direction of incidence and scattering as shown in Fig. 1.

---

[7] C. M. Crain, A. W. Straiton, and C. E. VonRosenberg, Trans. I.R.E., Vol. AP-1, No. 2, October, 1953.

[8] C. L. Staras, Jour. Appl. Phys., 23, 1152 (1952), has investigated the effect of other assumptions for $\rho(r)$ on scattering phenomena.

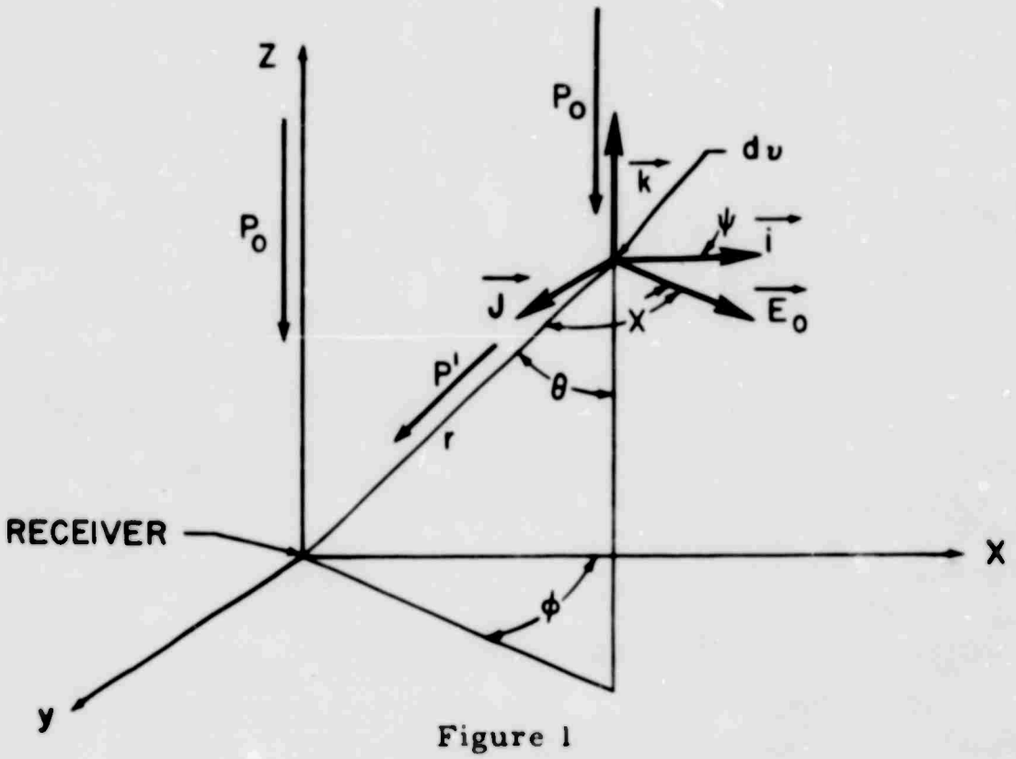

Figure 1

Coordinates for Turbulence Scattering of Vertically Incident Radiation

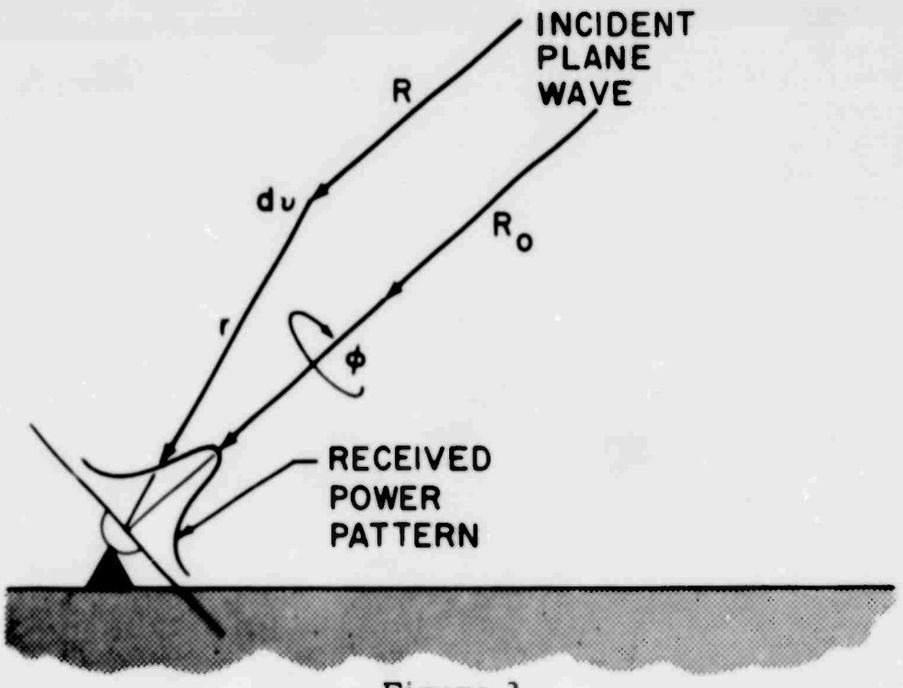

Figure 2

Multipath Propagation by Scattering

A. Scattered Wave

We shall consider first the energy scattered into a single antenna by off-axis turbulence clusters. The situation is pictured in Fig. (2) where the multipath propagation mode is clearly exhibited. The scattered waves give rise to an angular distribution of received power about the antenna's pointing axis, as indicated. The ratio of the power received by the antenna along the multipath (R + r) to that incident along the line-of-sight (R_o) for a scattering volume dv is

$$\frac{dP_s}{P_o} = \frac{R_o^2 \sigma(\theta, \phi)}{R^2 \cdot r^2} dv \qquad (2.4)$$

where σ denotes the scattering cross section per unit volume per unit solid angle. One may set $R_o = R$ for reasonably ($<4^o$) narrow beams and long range (>1000 m) transmission.

$$\frac{dP_s}{P_o} = \frac{\sigma(\theta, \phi)}{r^2} dv \, . \qquad (2.4a)$$

The path difference between the direct and multipath ray is simply

$$x = R + r - R_o \, . \qquad (2.5)$$

If one integrates (2.4a) over all volume elements satisfying this condition, the result may be interpreted as a "differential path difference power density," $dP_s = Q(x)\,dx$. The ratio of the scattered-to-direct power received with path difference x is thus:

$$\frac{Q(x)}{P_o} = \int dv \, \frac{\sigma(\theta, \phi)}{r^2} \delta(x + R_o - R - r) \, , \qquad (2.6)$$

where $\delta(z)$ is the familiar Dirac delta function.

(1) Phase Delay

Equation (2.6) may now be applied to predict an RMS phase error in a sinusoidal voltage at the receiving antenna. The anomolous propagation produces a linear superposition of scattered (and thus delayed) sinusoidal signals, as pictured in Fig. (3a). The resultant phase error (α) so produced may be inferred from the vector voltage diagram of Fig. (3b). The lag angle between the primary voltage E_o (assumed for the moment to be of constant phase) and scattered voltage $E(x)$ is $\theta = 2\pi x/\lambda$. The desired phase error α is computed as:

$$\alpha^2 = \int_o^\infty \frac{E^2(x)}{E_o^2} \sin^2\left(\frac{2\pi x}{\lambda}\right) dx ,$$

$$= \int_o^\infty dx \, \frac{Q(x)}{P_o} \sin^2\left(\frac{2\pi x}{\lambda}\right), \qquad (2.7)$$

in the approximation, $E(x) \ll E_o$. Introducing Eq. (2.6), the mean squared error becomes:

$$\langle \alpha^2 \rangle = \int_o^\infty dx \sin^2\left(\frac{2\pi x}{\lambda}\right) \int dv \, \frac{\sigma(\theta,\phi)}{r^2} \, \delta\left[x + R_o - R - r\right] . \qquad (2.8)$$

The primed volume integration restricts that process to the admittance angle (i.e., beamwidth) of the receiving antenna. This step is a crucial one, since widening that angle indefinitely would only serve to include all scattering elements within sight, and so produce a divergent answer. The spherical shape of the earth and limited (height) extent of the turbulence reduces such an accumulation in actual experiments. One must also consider the

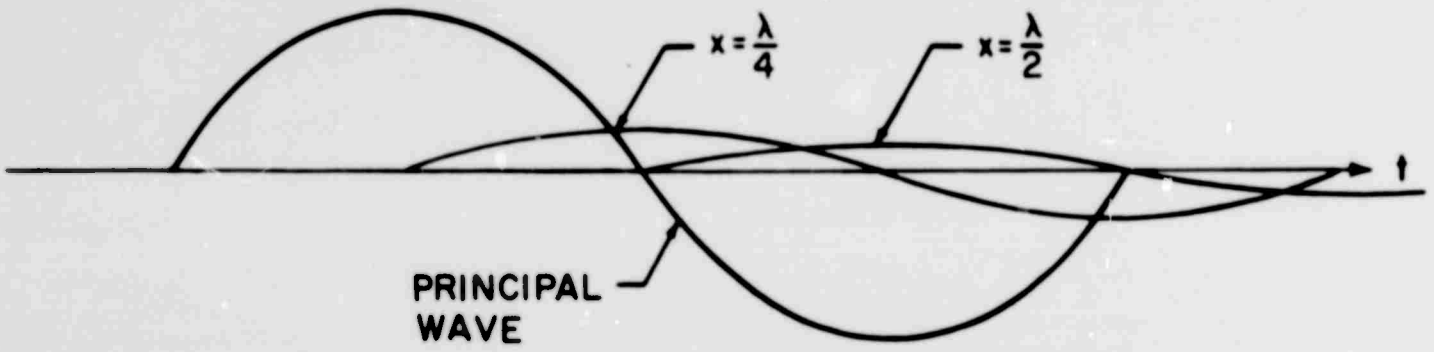

(a)

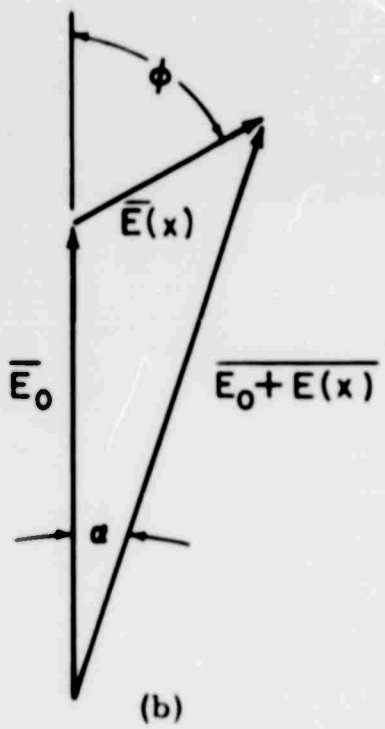

(b)

Figure 3

Superposition of Multipath Signals
(a) Principal Wave Plus Delayed-Scattered Signals
(b) Vector Voltage Diagram

attenuation of the scattered waves for a complete treatment. We shall avoid such considerations by exploiting the characteristically small beamwidths of radar receivers as a natural cut-off.

To compute the integrals appearing in Eq. (2.8), we erect a spherical coordinate system on the receiving antenna's pointing direction, as shown in Fig. 2. If β is the antenna beamwidth and L the transmission range through the troposphere,

$$\left\langle a^2 \right\rangle = \int_0^\infty dx \sin^2\left(\frac{2\pi x}{\lambda}\right) \int_0^L dr \int_0^\beta d\theta \sin\theta \int_0^{2\pi} d\phi \, \sigma(\theta,\phi)\delta\left[x - r(1 - \cos\theta)\right]. \tag{2.9}$$

We must now express $\sigma(\theta, \phi)$ in terms of θ and ϕ.

$$\sigma(\theta,\phi) = \frac{4 \left\langle \Delta N^2 \right\rangle 10^{-12}}{\lambda} \cdot \frac{\left(\frac{2\pi \ell_o}{\lambda}\right)^3 \left[1 - \sin^2(\theta)\cos^2(\phi - \psi)\right]}{\left[1 + 2\left(\frac{2\pi \ell_o}{\lambda}\right)^2 (1 - \cos\theta)\right]^2}. \tag{2.10}$$

The definition of the dielectric constant in terms of the index of refraction (i.e., $\epsilon = n^2$) and the N-unit notation, $\Delta N = (n - 1)10^6$ are here utilized. All but one of the integrations in Eq. (2.9) may be performed analytically if one disregards altitude variations in ℓ_o and ΔN^2 — a procedure which is certainly consistent with our other approximations.

$$\left\langle a^2 \right\rangle \simeq \left\langle \Delta N^2 \right\rangle 10^{-12} \cdot \left(\frac{2\pi \ell_o}{\lambda}\right)^3 \int_0^U du \, \frac{\left(1 - \frac{\sin(u)}{u}\right)^2}{\left[1 + \frac{2\pi \ell_o^2}{\lambda L} \cdot u\right]^2} \tag{2.11}$$

where

$$U = \frac{4\pi L}{\ell_o}(1 - \cos\beta).$$

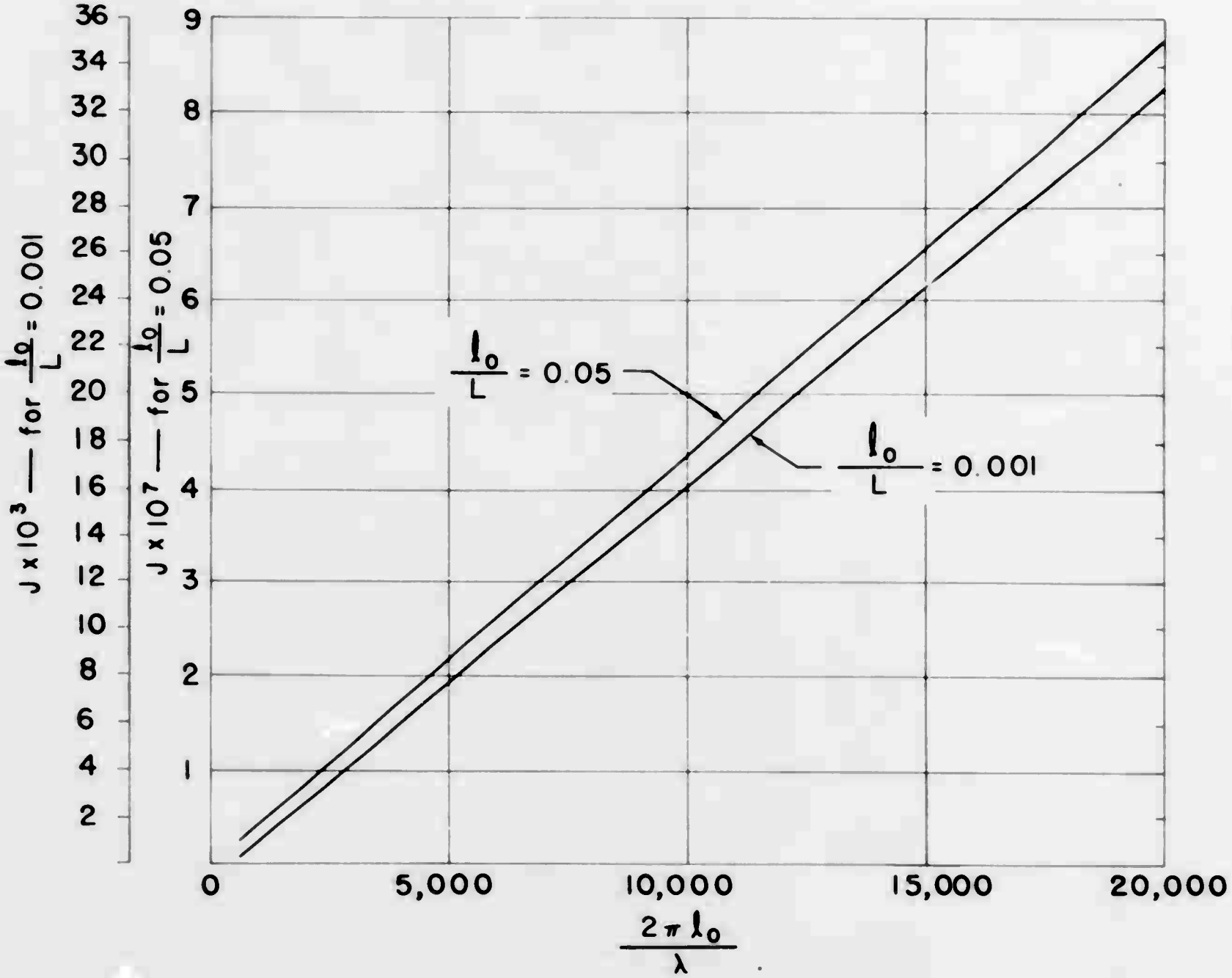

Figure 4

RMS Phase Error for Scattered Component

The ratio $\frac{\langle a^2 \rangle}{\langle \Delta N^2 \rangle}$ is plotted in Fig. (4) as a function of $2\pi\ell_o/\lambda$ for various L/ℓ_o.

(2) Angular Distribution

The angular distribution of scattered power about the receiving antenna's pointing direction may be extracted from Eq. (2.6) by integrating over all path differences x. Again using an antenna-centered spherical coordinate system.

$$\frac{\langle |E_s|^2 \rangle}{|E_o|^2} = \int_o^\infty dx \, \frac{Q(x)}{P_o} ,$$

$$= \int_{\cos\beta}^1 d(\cos\theta) \int_o^L dr \int_o^{2\pi} d\phi \, \sigma(\theta, \phi) , \qquad (2.12)$$

where $\sigma(\theta, \phi)$ is given by Eq. (2.10). The angular power distribution is recognized as the $d(\cos\theta)$ integrand in Eq. (2.12), so that

$$\frac{1}{P_o} \frac{dP_s}{d(\cos\theta)} = \frac{2L}{\ell_o} \left(\frac{2\pi\ell_o}{\lambda}\right)^4 \langle \Delta N^2 \rangle \, 10^{-12} \, \frac{1 + \cos^2(\theta)}{\left[1 + 2\left(\frac{2\pi\ell_o}{\lambda}\right)^2 (1 - \cos\theta)\right]^2} , \qquad (2.13)$$

where constancy of the scattering parameters, ℓ_o and $\langle \Delta N^2 \rangle$, over the transmission path has again been assumed. The distribution, Eq. (2.13), is plotted in Fig. (5) as a function of θ for various $2\pi\ell_o/\lambda$. In the region $0 < \theta < \frac{\lambda}{2\pi\ell_o} \simeq 10^{-3}$, the denominator is sensibly unity and the density equals

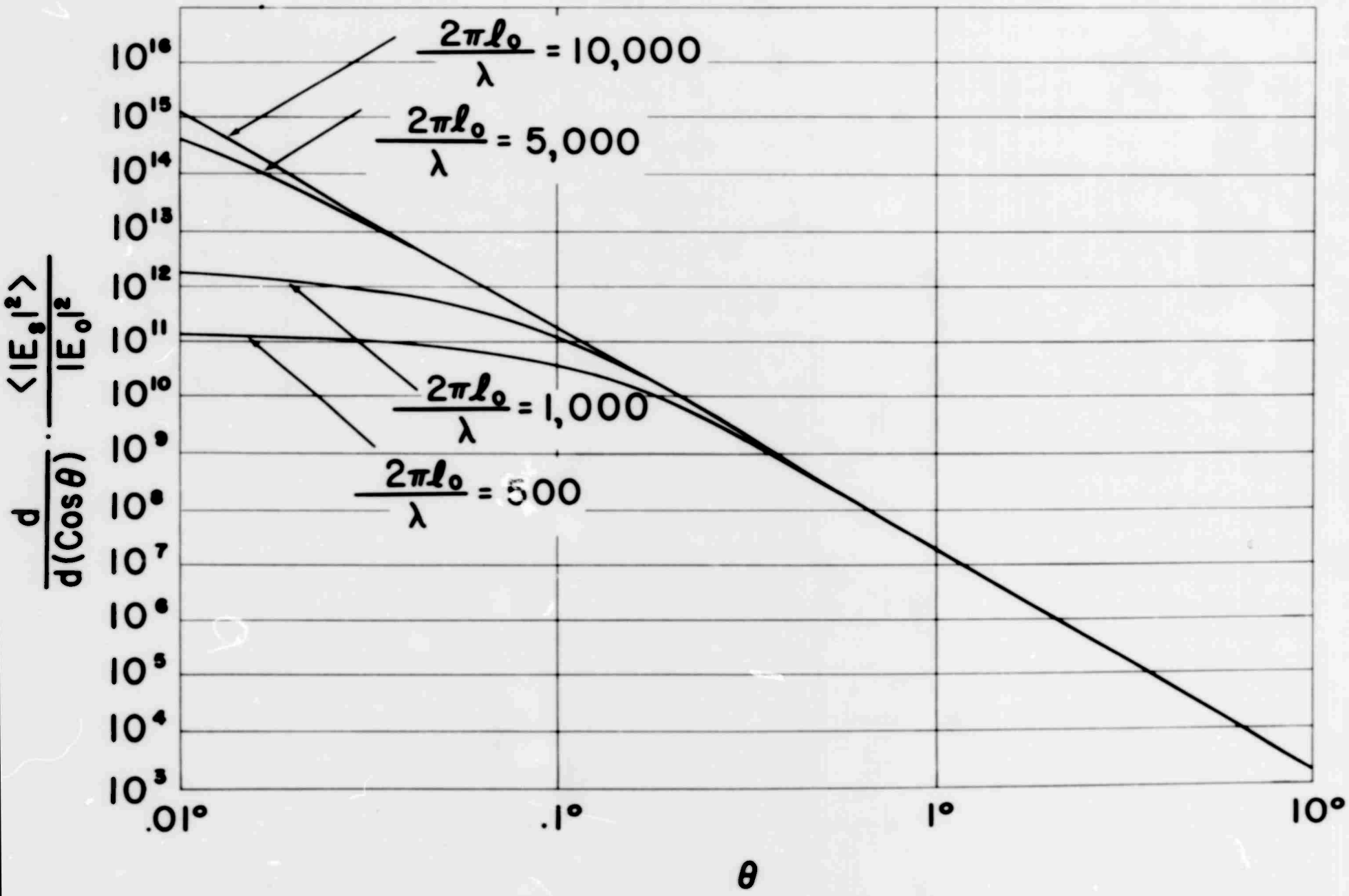

Figure 5

Angular Distribution for Turbulence Scattering

$2 \cdot \left(\frac{2\pi \ell_o}{\lambda}\right)^4$. For larger angles, it falls off rapidly, reaching 1/4 at right angles to the beam.

The result, Eq. (2.13), may be further refined by including the effect of attenuation of the scattered signals in reaching the antenna from the various volume elements. LaGrone, Benson, and Straiton[9] have computed the energy which is removed from a beam per mile with the same theory of tropospheric turbulence scattering used here. Their result is

$$\frac{db}{mile} = 6983\left(\frac{4\pi}{\lambda}\right)\left\langle \Delta N^2 \right\rangle 10^{-12} \left(\frac{2\pi \ell_o}{\lambda}\right). \qquad (2.14)$$

In evaluating Eq. (2.12) one should thus include a range-dependent absorption factor

$$\frac{\left\langle |E_s|^2 \right\rangle}{|E_o|^2} \simeq \int_{\cos\beta}^{1} d(\cos\theta) \int_o^L dr \int_o^{2\pi} d\phi \cdot \sigma(\theta,\phi)\, e^{-r\left[700 \frac{4\pi}{\lambda} \left\langle \Delta N^2 \right\rangle 10^{-12} \left(\frac{2\pi \ell_o}{\lambda}\right)\right]} \qquad (2.15)$$

The attenuation effect is almost completely negligible in this case, since forward scattering is so favored by the cross section, Eq. (2.3).

B. The Direct Wave

The preceding discussion was concerned only with the scattered wave. As in any scattering problem, the resulting field at a point in space is composed of both the direct and scattered wave. In the present instance, however, the direct wave cannot be written as a simple sinusoidal plane wave since it has traversed a region of random and variable delay.

---

[9] Jour. Appl. Physics, 22, 672 (1951).

(1) Phase Delay

To compute the phase delay suffered in traversing a length L of turbulence, we shall write the received electric field (E_R) in exponential form.[10]

$$E_R = E_T \exp\left[i2\pi f \int_o^L \frac{d\ell}{v_e}\right] . \qquad (2.16)$$

E_T is the transmitted field strength and f the frequency. The velocity of propagation (v_e) depends on the dielectric constant and so is a function of position along the path. If we separate a random portion from the dielectric constant, $e = e_o + \Delta e$, we can rewrite Eq. (2.16) as,

$$E_R = E_T \exp i\left[\frac{2\pi}{\lambda} L + \frac{\pi}{\lambda} \int_o^L d\ell \frac{\Delta e(\ell)}{e_o}\right] . \qquad (2.17)$$

The random part of the phase angle is represented by the exponent's second term. Calling this a and taking the mean square,

$$\langle a^2 \rangle = \frac{\pi^2}{\lambda^2} \int_o^L d\ell_1 \int_o^L d\ell_2 \left\langle \frac{\Delta e^*(\ell_1)}{e_o^*} \cdot \frac{\Delta e(\ell_2)}{e_o} \right\rangle . \qquad (2.18)$$

The integrand is just $\left\langle \left|\frac{\Delta e}{e}\right|^2 \right\rangle \rho(\ell_1 - \ell_2)$ by our definition Eq. (2.1), so that one has

$$\langle a^2 \rangle = \frac{\pi^2 \left\langle \left|\frac{\Delta e}{e}\right|^2 \right\rangle}{\lambda^2} \int_o^L d\ell_1 \int_o^L d\ell_2 \exp\left[-(\ell_1 - \ell_2)/\ell_o\right] ,$$

(continued on following page)

(10) See also J. Feinstein, Trans. I.R.E., PGAP, Vol. AP-2, 63 (1954).

$$= \frac{8\pi^2 \ell_o^2 \langle \Delta N^2 \rangle 10^{-12}}{\lambda^2} \left(\frac{L}{\ell_o} \right) , \qquad (2.19)$$

for the mean square phase deviation of the direct wave.

To determine the time spectrum for this turbulence, consider a mass of turbulent air moving with an average velocity v. Take a set of coordinates also moving with the mass (i.e., at speed v). Measurements of fluctuations in this moving system will give data from which the time spectrum can be calculated. Unfortunately, such data are not available and in their absence an approximate treatment must be used. In the following we shall calculate the time spectrum produced by a line-of-sight, rotating through a turbulent air mass containing variations which are not changing in time relative to one another. This is equivalent to assuming that the line-of-sight moves through a characteristic length ℓ_o in a time short compared to the time of significant change in the turbulence pattern. In Part IV we shall consider the analogous problem of the line-of-sight moving parallel to itself. That this procedure will yield useful results is suggested by some experiments performed by Straiton and Smith.[11]

A rotating line-of-sight sweeps through an angle $\theta = \tau\dot{\theta}$ in time τ, where $\dot{\theta}$ is the angular rate. (See Fig. 6.) Defining α as before, one can write

$$\langle \alpha(t)\alpha(t+\tau) \rangle = \frac{\pi^2}{\lambda^2} \int_o^{L_1} d\ell_1 \int_o^{L_2} d\ell_2 \frac{\langle \Delta\epsilon^*(x_1, y_1)\, \Delta\epsilon(x_2, y_2) \rangle}{|\epsilon|^2} \qquad (2.20)$$

[11] A. W. Straiton and H. W. Smith, Proc. I.R.E., 38, 825 (1950).

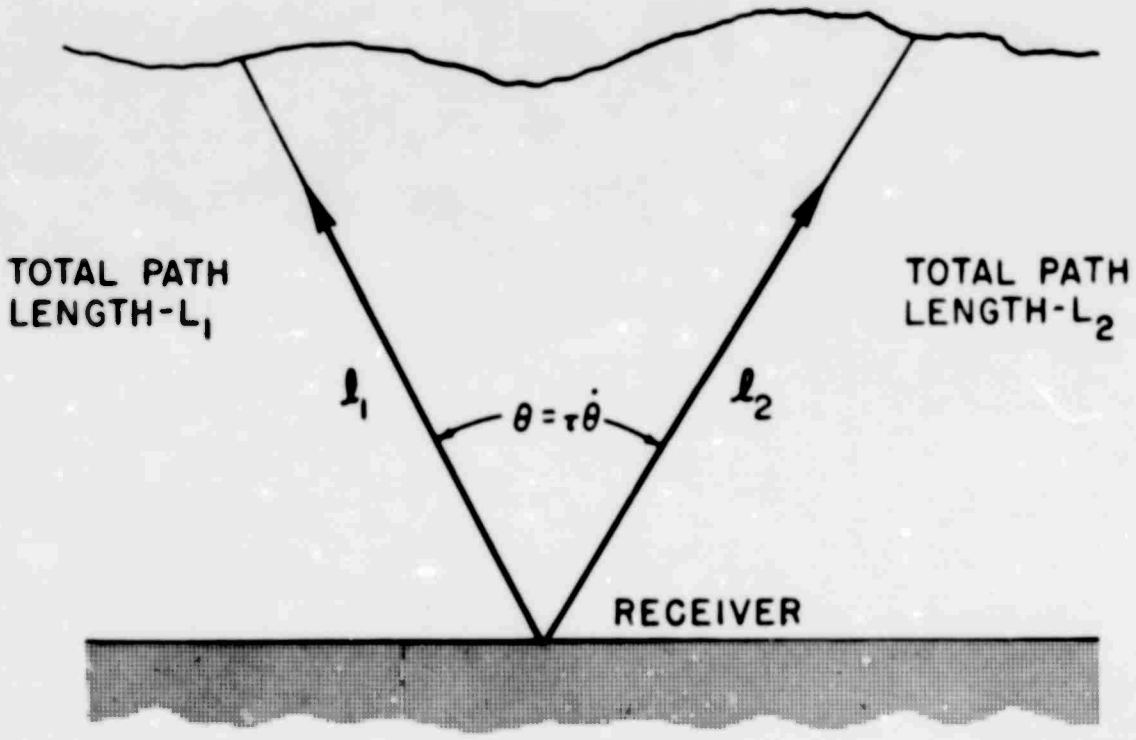

Figure 6

Geometry for Rotating Line-of-Sight

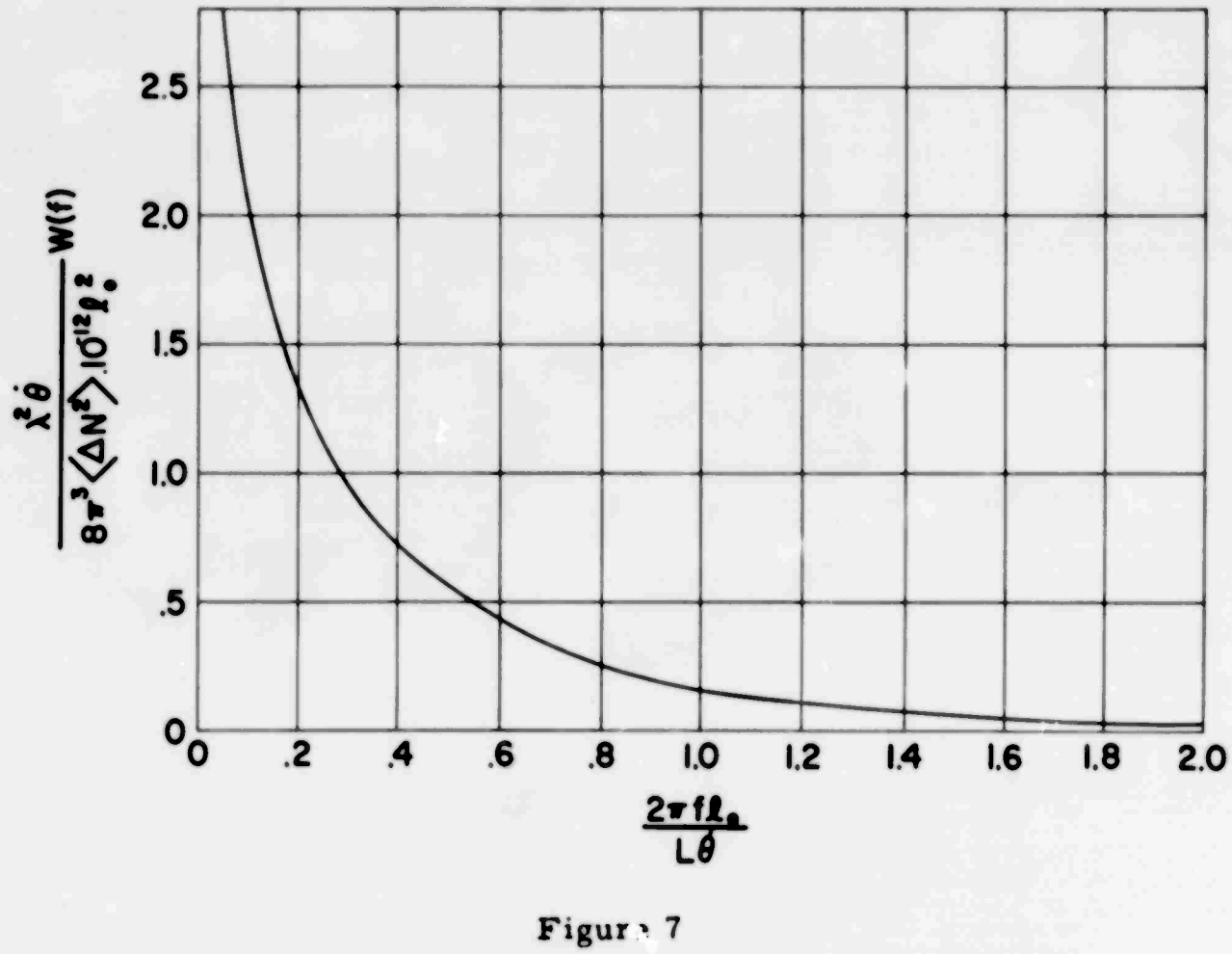

Figure 7

Power Spectrum of Phase for Rotating Line-of-Sight

where the first integral is taken along path ℓ_1 at time t, and the second along line ℓ_2 at τ seconds later. Using Eq. (2.2) and measuring distance along the line-of-sight from the origin, Eq. (2.20) can be written

$$\left\langle a(t)a(t+\tau)\right\rangle = \frac{4\pi^2\left\langle \Delta N^2\right\rangle 10^{-12}}{\lambda^2}\int_o^{L_1} d\ell_1 \int_o^{L_2} d\ell_2$$

$$\cdot \exp\left(-\frac{1}{\ell_o}\sqrt{\ell_1^2+\ell_2^2-2\ell_1\ell_2\cos\theta}\right). \qquad (2.21)$$

It is convenient to assume that $L_1 \cong L_2$, (i.e., that the path is long compared to any changes in length), so that Eq. (2.21) can be changed to polar coordinates and integrated once to yield:

$$\left\langle a(t)a(t+\tau)\right\rangle = \frac{8\pi^2\left\langle \Delta N^2\right\rangle 10^{-12}\ell_o^2}{\lambda^2}\int_o^{\pi/4} d\phi \left\{\frac{1}{1-\sin 2\phi\cos\theta}\right.$$

$$\left. - \frac{L\exp\left[-\frac{L\sqrt{1-\sin 2\phi\cos\theta}}{\ell_o\cos\phi}\right]}{\ell_o\cos\phi\sqrt{1-\sin 2\phi\cos\theta}} - \frac{\exp\left[-\frac{L\sqrt{1-\sin 2\phi\cos\theta}}{\ell_o\cos\phi}\right]}{1-\sin 2\phi\cos\theta}\right\}. \qquad (2.22)$$

The first term is readily integrated again. If $L/\ell_o \gg 1$, the last two terms make significant contributions only for $\theta \ll \pi/2$ and $\phi \cong \pi/4$. One may put

$$\sin 2\phi \cong 1 - \frac{\left(2\phi - \frac{\pi}{2}\right)^2}{2}, \qquad \cos\phi \cong \frac{1}{\sqrt{2}}, \qquad (2.23)$$

and with the substitution

$$\phi = \sqrt{\frac{1-\cos\theta}{2\cos\theta}}\sqrt{y^2-1} + \frac{\pi}{4}, \qquad (2.24)$$

the second term in Eq. (2.22) becomes

$$\int_0^{\pi/4} d\phi \frac{L \exp\left[-\frac{L\sqrt{1 - \sin 2\phi \cos\theta}}{\ell_o \cos\phi}\right]}{\ell_o \cos\phi \sqrt{1 - \sin 2\phi \cos\theta}} \cong \frac{L}{\ell_o\sqrt{\cos\theta}} \int_1^Y dy \frac{\exp\left[-\frac{\sqrt{2(1 - \cos\theta)}\, Ly}{\ell_o}\right]}{\sqrt{y^2 - 1}} \tag{2.25}$$

where

$$Y = \sqrt{\frac{\pi^2 \cos\theta}{8(1 - \cos\theta)} + 1}\,. \tag{2.26}$$

When $L/\ell_o >> 1$ and $\theta << \pi/2$, one can put $Y = \infty$ with small error. The integral thus becomes

$$\frac{L}{\ell_o} \int_1^\infty dy \frac{\exp\left[-\frac{|\theta| Ly}{\ell_o}\right]}{\sqrt{y^2 - 1}} = \frac{L}{\ell_o} K_o\left(\frac{|\theta| L}{\ell_o}\right), \tag{2.27}$$

where K_o is a modified Bessel function of the second kind. The last term can be treated in a similar fashion.

$$\frac{1}{|\theta|} \int_1^\infty dy \frac{\exp\left[-\frac{|\theta| Ly}{\ell_o}\right]}{y\sqrt{y^2 - 1}} = \frac{1}{|\theta|} \int_{\frac{|\theta| L}{\ell_o}}^\infty d\eta \int_1^\infty dy \frac{\exp[(-\eta y)]}{\sqrt{y^2 - 1}} = -\frac{\pi}{2|\theta|}$$

$$+ \frac{\pi L}{2\ell_o}\left[K_o\left(\frac{|\theta| L}{\ell_o}\right) L_{-1}\left(\frac{|\theta| L}{\ell_o}\right) + K_1\left(\frac{|\theta| L}{\ell_o}\right) L_o\left(\frac{|\theta| L}{\ell_o}\right)\right]. \tag{2.28}$$

L_μ denotes the modified Struve function. Combining all of these results, one finds:

$$\left\langle a(t)a(t+\tau)\right\rangle = \frac{8\pi^2 \ell_o^2 \left\langle \Delta N^2 \right\rangle 10^{-12}}{\lambda^2} \left(\frac{L}{\ell_o}\right) \left\{ \frac{\pi}{2} \left[K_o\left(\frac{|\theta| L}{\ell_o}\right) L_{-1}\left(\frac{|\theta| L}{\ell_o}\right) + K_{-1}\left(\frac{|\theta| L}{\ell_o}\right) L_o\left(\frac{|\theta| L}{\ell_o}\right) \right] - K_o\left(\frac{|\theta| L}{\ell_o}\right) \right\} \qquad (2.29)$$

where $\theta = \dot{\theta}\tau$. When $\tau = 0$, Eq. (2.29) reduces to Eq. (2.19).

The spectrum may be found by taking the cosine transform of Eq. (2.29)

$$W(f) = \int_{-\infty}^{\infty} d\tau \cos 2\pi f\tau \left\langle a(t)a(t+\tau)\right\rangle . \qquad (2.30)$$

Upon substituting Eq. (2.29) into Eq. (2.30), the second term may be integrated directly. The first term may be simplified by using the identity

$$\frac{1}{z}\left[1 - \frac{2}{\pi} \int_z^{\infty} K_o(x)\, dx\right] = K_o(z) L_{-1}(z) + K_{-1}(z) L_o(z) .$$

The integral to be evaluated can then be written

$$\frac{2\ell_o}{L\dot{\theta}} \int_o^{\infty} du \frac{\cos \omega_1 u}{u} \left[1 - \frac{2}{\pi} \int_u^{\infty} K_o(x)\, dx\right] \qquad (2.31)$$

where $\omega_1 = 2\pi f \ell_o / L\dot{\theta}$. Equation (2.31) may be integrated once by parts to give

$$\frac{4\ell_o}{\dot{\theta}L} \int_o^{\infty} du\, K_o(u) \int_{\omega_1 u}^{\infty} \frac{\cos t}{t} dt . \qquad (2.32)$$

By changing the variable in the second integral to $y = t/\omega_1 u$, the order of integration may be reversed whereupon the remaining integrations may be performed directly. The complete result is

$$W(f) = \frac{8\pi^3 \cdot 10^{-12} \langle \Delta N^2 \rangle \ell_o^2}{\lambda^2 \dot{\theta}} \left[\log \frac{1 + \sqrt{1 + w_1^2}}{w_1} - \frac{1}{\sqrt{1 + w_1^2}} \right] . \qquad (2.33)$$

This is plotted on Fig. 7.

(2) Fluctuations in Angle of Arrival

In addition to the phase delay suffered in traversing the troposphere, the direct ray will exhibit a random variation in angle of arrival at the receiver. This effect is analogous to the angular scintillations of star images[12] and is produced by gradients in the index of refraction at right angles to the ray path. The equation governing propagation of a ray through a variable medium according to Fermat's principle is,[13]

$$\frac{d}{d\ell}(\eta \vec{t}) - \vec{\nabla} \cdot \eta = 0 , \qquad (2.34)$$

where $\vec{t}$ is a unit vector along the ray, ℓ is the distance along the ray and n is the index of refraction. Equation (2.34) can be rearranged to read,

$$\frac{d\vec{t}}{d\ell} = \vec{\nabla}\left[\log (\eta)\right] - \vec{t}\left(\vec{t} \cdot \vec{\nabla}\left[\log (\eta)\right]\right) . \qquad (2.35)$$

To evaluate these operations, introduce the decompositions:

$$\eta = \eta_o + N_1 \qquad \text{and} \qquad \vec{t} = \vec{t}_o + \vec{\epsilon} , \qquad (2.36)$$

where $\vec{t}_o$ is the initial value of $\vec{t}$, η_o is the mean index of refraction and is very

---

[12] S. Chandrasekhar, Monthly Notices, Royal Astro. Soc., 112, 475 (1952). See also H. W. Liepmann, "Reflection and Diffusion of a Light Ray Passing Through a Boundary Layer," Douglas Aircraft Co., Inc., Rpt SM-14397, May 16, 1952, for a discussion of a similar phenomenon.

[13] D. Kerr, "Propagation of Short Radio Waves," Rad. Lab. Series, Vol. 13, McGraw-Hill, 1951, page 44.

nearly equal to unity, and N_1 is the variable part of η.* To first order in e and N_1 (which must be very small), Eq. (2.35) can be written,

$$\frac{d\vec{\epsilon}}{d\ell} = \vec{\nabla} N_1 - \hat{r}_o \frac{\partial N_1}{\partial \ell} . \tag{2.37}$$

$d\vec{\epsilon}/d\ell$ defines a differential angle (and direction) of ray displacement. Equation (2.37) gives this angle in terms of the gradient normal to the path; integrating over the whole path gives the total angular deflection.

Let us return to the rotating line-of-sight problem. Using cylindrical coordinates (with the z-axis normal to the page), the orthogonal components of angle deviation obtained from Eq. (2.37) are:

$$\phi_z = \int_o^L d\ell \frac{\partial N_1}{\partial z} \tag{2.38}$$

$$\phi_\theta = \int_o^L d\ell \frac{1}{\ell} \frac{\partial N_1}{\partial \theta} . \tag{2.39}$$

The auto-correlations of these two functions are thus:

$$\langle \phi_z(t)\phi_z(t+\tau) \rangle = \int_o^L d\ell_1 \int_o^L d\ell_2 \left\langle \left.\frac{\partial N}{\partial z}\right|_1 \left.\frac{\partial N}{\partial z}\right|_2 \right\rangle \tag{2.40}$$

$$\langle \phi_\theta(t)\phi_\theta(t+\tau) \rangle = \int_o^L d\ell_1 \int_o^L d\ell_2 \frac{1}{\ell_1 \ell_2} \left\langle \frac{\partial N}{\partial \theta_1} \frac{\partial N}{\partial \theta_2} \right\rangle \tag{2.41}$$

Considering Eq. (2.40) first, we have by differentiating inside the average signs in the definition of ρ,

$$\left\langle \left.\frac{\partial N_1}{\partial z}\right|_1 \left.\frac{\partial N_1}{\partial z}\right|_2 \right\rangle = - \langle N_1^2 \rangle \cdot \frac{\partial^2 \rho(r_{12})}{\partial \xi^2} \tag{2.42}$$

*In terms of N units, $N_1 = \Delta N \cdot 10^{-6}$.

with r_{12} given by Eq. (2.43) below and ξ equal to $z_2 - z_1$. In cylindrical coordinates, the distance between two general points (1) and (2) is:

$$r_{12} = \left[\ell_1^2 + \ell_2^2 - 2\ell_1\ell_2\cos(\theta_2 - \theta_1) + (z_2 - z_1)^2\right]^{1/2} . \qquad (2.43)$$

Evaluating Eq. (2.42) in the x, y plane ($z_1 = z_2 = 0$), one obtains

$$\left\langle \left.\frac{\partial N_1}{\partial z}\right|_1 \left.\frac{\partial N_1}{\partial z}\right|_2 \right\rangle_{\substack{z_1=0 \\ z_2=0}} = -\langle N_1^2\rangle \frac{1}{r_{12}} \frac{d\rho(r_{12})}{dr_{12}} . \qquad (2.44)$$

Using Eq. (2.2) and taking $\theta_1 = 0$, we have

$$\langle \phi_z(t)\phi_z(t+\tau)\rangle = \frac{\langle N_1^2\rangle}{\ell_o} \cdot \int_o^L d\ell_1 \int_o^L d\ell_2 \frac{e^{-\frac{\left[\ell_1^2 + \ell_2^2 - 2\ell_1\ell_2\cos(\theta)\right]^{1/2}}{\ell_o}}}{\left[\ell_1^2 + \ell_2^2 - 2\ell_1\ell_2\cos\theta\right]^{1/2}} . \qquad (2.45)$$

The methods used in integrating Eq. (2.21) may be applied here to yield

$$\langle \phi_z(t)\phi_z(t+\tau)\rangle = \pi\langle \Delta N^2\rangle \cdot 10^{12} \cdot \frac{L}{\ell_o}\left[K_o(\mu)L_{-1}(\mu) + K_{-1}(\mu)L_o(\mu)\right] \qquad (2.46)$$

with

$$\mu = \frac{L\dot{\theta}|\tau|}{\ell_o} .$$

It will be noted that Eq. (2.46) becomes infinite as $\tau \longrightarrow 0$; which is to say, the mean square deviation of ϕ_r is infinite. This is simply a consequence of our choice for the correlation function made in Eq. (2.2). Unfortunately, Eq. (2.2) describes a (Markov) process which has no derivatives. This need not disturb one unduly, since a spectrum can still be found from Eq. (2.46) by taking its cosine transform. The spectrum $W_r(f)$ obtained from the cosine

Figure 8 Rotating Line-of-Sight Angle of Arrival Spectra for

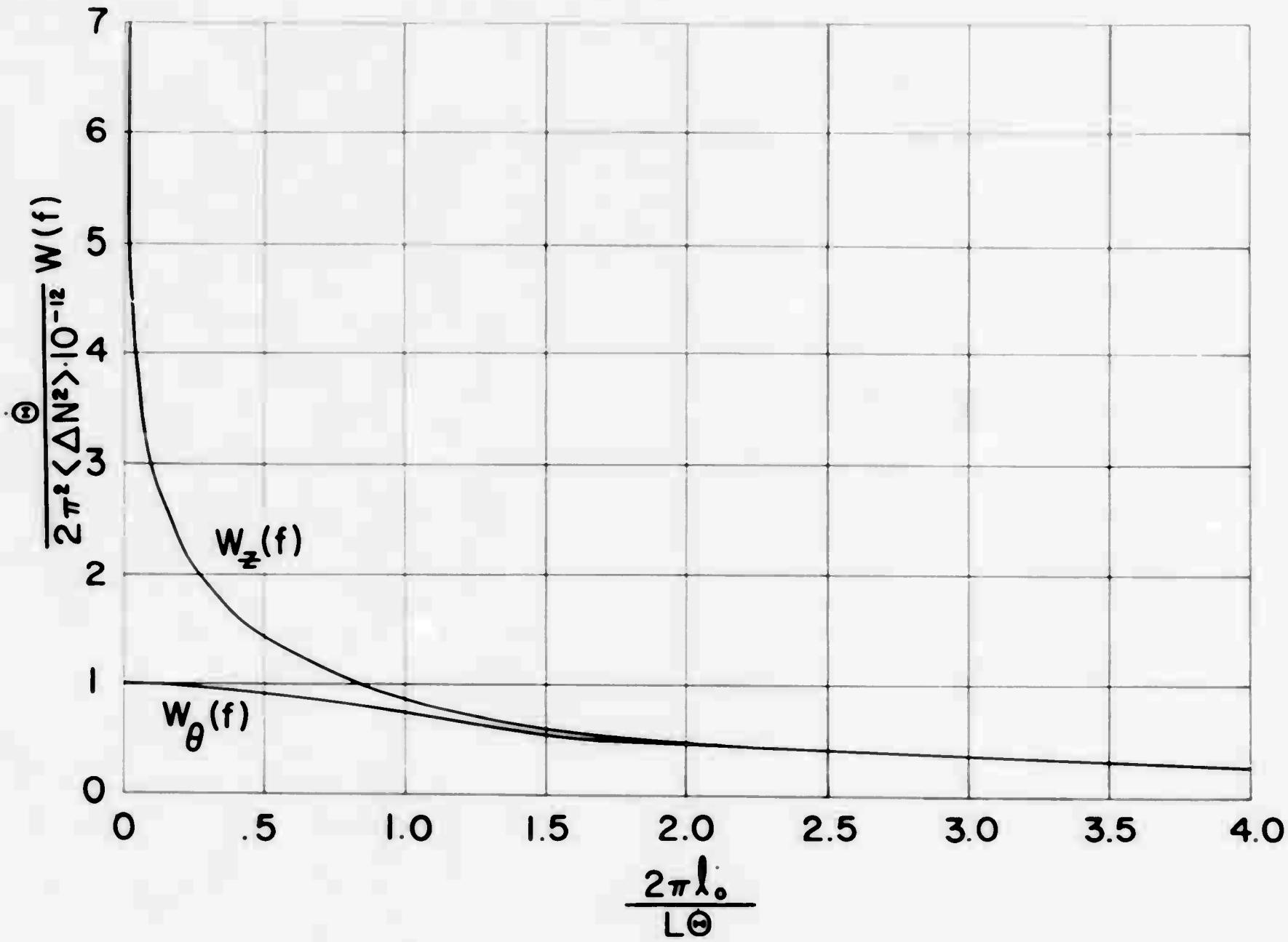
7
6
5
4
3
2
1
0
$\frac{\Theta}{2\pi^2\langle\Delta N^2\rangle\cdot 10^{-12}}$ W(f)
$W_z(f)$
$W_\theta(f)$
0
.5
1.0
1.5
2.0
2.5
3.0
3.5
4.0
$\frac{2\pi l_o}{L\Theta}$

transform of Eq. (2.46) is

$$W_z(f) = \frac{2\pi \cdot 10^{-12} \langle \Delta N^2 \rangle}{\dot{\theta}} \log \frac{1 + \sqrt{1 + w_1^2}}{w_1} \qquad (2.47)$$

with w_1 defined as in Eq. (2.31). This is plotted in Fig. 8. This spectrum is meaningful, except as the frequency $f \rightarrow \infty$. The behavior at large f is such that $\int_{-\infty}^{\infty} df\, W(f)$ diverges, yet the density at low frequencies is correct. Since the data are too crude to indicate a better choice for $\rho(r)$, we have tried to extract the maximum amount of usable information from Eq. (2.2). A different choice for $\rho(r)$ might well give a spectrum whose integral converges, yet the low frequency density would not be more trustworthy than that derived from Eq. (2.47). One might thus be led to a false sense of security in calculating the total mean square as a definite number; when, in fact, slight variations in $\rho(r)$, which might fit the data equally well, could produce large changes in $\langle \phi_r^2 \rangle$.

The auto-correlation of ϕ_θ and the corresponding spectrum can be found by a procedure similar to that above.

$$\langle \phi_\theta(t) \phi_\theta(t + \tau) \rangle = 2 \cdot 10^{-12} \langle \Delta N^2 \rangle \frac{L}{\ell_o} K_o \left[\frac{L\dot{\theta}|\tau|}{\ell_o} \right], \qquad (2.48)$$

and

$$W_\theta(f) = \frac{2\pi^2 \cdot 10^{-12} \langle \Delta N^2 \rangle}{(\dot{\theta})^2} \cdot \frac{1}{\left[1 + \left(\frac{2\pi f \ell_o}{\dot{\theta} L} \right)^2 \right]^{1/2}}. \qquad (2.49)$$

Equation (2.49) is also plotted in Fig. 8.

C. Probability Densities

(1) Total Field Strength

In the derivation[1] of Eq. (2.3) it is assumed that the volume elements to which the equation applies are large in linear dimensions compared to ℓ_o. When this is true, the scattering from separate volume elements will have random phasing. The total field is the sum of these scattered fields and its amplitude will be Rayleigh distributed. The direct ray has random phase but constant amplitude. The sum of direct and scattered waves is then the sum of a sine wave plus Gaussian noise and has the well known form,[14][15]

$$p(E) = \frac{E}{Q} \exp\left[-\frac{E^2 + P^2}{2Q}\right] I_o\left(\frac{EP}{Q}\right). \qquad (2.50)$$

Here p(E) is the probability density of finding the sum amplitude E between E and E + dE, Q is the total scattered power, P is the direct wave amplitude, and $I_o(x)$ is a modified Bessel function of the first kind. The case $P \gg Q$, which is of interest here, allows Eq. (2.50) to be reduced to

$$p(E) \cong \frac{1}{\sqrt{2\pi Q}} \exp\left[-(E - P)^2/2Q\right] . \qquad (2.51)$$

This shows that the received amplitude will be very nearly normally distributed, with mean P and standard deviation $Q^{1/2}$.

(2) Phase Angle Probability Densities

As just stated above, the phases of the scattered waves will be random, i.e., α is uniformly distributed from $-\pi$ to π. This must be combined with the phase deviation of the direct ray. From Eq. (2.17), the total phase delay is

---

[14] Rice, Mathematical Analysis of Random Noise, BSTJ, 24, 46 (1945).
[15] Lawson and Uhlenbeck, Threshold Signals, Rad. Lab. Series, 24, McGraw-Hill (1950).

given as the sum of the individual phase delays in the turbulence clusters. The sum will be normally distributed by virtue of the central limit theorem.[16] This theorem predicts a normal density function over an infinite range for phase; in the more usual case where phase is considered modulo 2π, the resulting density function is[17]

$$p(a) = \frac{1}{2\pi}\,\theta_3\left(\frac{a}{2\pi}, \frac{\langle a^2\rangle}{2\pi}\right) \tag{2.52}$$

where θ_3 is a theta-function. When $(\langle a^2\rangle)^{1/2} \ll 2\pi$, this reduces to the normal form

$$p(a) = \frac{1}{\sqrt{2\pi\langle a^2\rangle}}\, e^{-\frac{a^2}{2\langle a^2\rangle}} . \tag{2.53}$$

The angle of arrival density for the scattered wave is given by Eq. (2.13). The ray deviation density will be normal in two dimensions (and uncorrelated in those two dimensions).

D. Numerical Estimates

Some estimates have been made for the scattering parameters which appear in the foregoing expressions. Very near the ground,[18] one finds $\Delta N \simeq 10$. Microwave refractometer flights[2] indicate that ΔN varies between 1/2 and 1N units from several hundred to thirty-thousand feet. This altitude range includes most of the tropospheric region in which refractive fluctuations affect propagation. The correlation length ℓ_o has a ground level value of 20

---

[16] H. Cramer, "Mathematical Methods of Statistics," Princeton University Press, 1946.

[17] P. Levy, Societe Math. de France, Comptes Rendus, p. 32, 1938.

[18] C. M. Crain and J. R. Gerhardt, Proc. I.R.E., 40, 50 (1952).

feet and increases rapidly to an asymptotic value of one or two hundred feet. Since the precise values of ℓ_o and ΔN vary with both geographic location and time, we shall choose the convenient averages: $\Delta N = 1/2$ and $\ell_o = 100$ feet. We take our line-of-sight transmission path length L to be 10,000 feet and assume an antenna beamwidth β of 3^o. We shall also take $\lambda = 6$ cm so as to (later) validate the Rayleigh approximation and avoid the attenuation problems characteristic of shorter wavelengths.

Contributions to the RMS phase error arise from both the scattered and direct wave. Substituting the above parameters into Eq. (2.11) and Eq. (2.19), we find:

$$\left\langle a_{sc}^2 \right\rangle = 2.5 \cdot 10^{-3} \text{ radians}^2 ,$$

and

$$\left\langle a_{direct}^2 \right\rangle = 0.5 \cdot 10^{-1} \text{ radians}^2 . \qquad (2.54)$$

Scintillation of the direct wave is evidently the dominant effect here. This error represents one-tenth of a cycle at 5,000 Mcs, thereby posing a genuine problem for systems requiring high phase stability over the transmission path.

The spectrum of such phase fluctuations is of considerable interest also. Since the characteristic turbulent self-motions (and hence doppler shifts) are known only in terms of the qualitative picture of eddy degeneration (Refs. (3) and (4)), we have computed spectra for a moving line-of-sight. We have just considered a rotating path, the spectrum of which is given in Figure 7. A measure of spectral width is given by $2\pi f \ell_o / L\dot{\theta} = 1$. If one assumes that the line-of-sight is rotating so as to track an aircraft flying 1,000 fps at an altitude of 10,000 feet (overhead), $\dot{\theta}$ is approximately 0.1 radians/sec. Using

this with the parameters above, the effective width is 1.59 cps.

A somewhat different model is obtained by anticipating the result of Part IV which gives the spectrum for a line-of-sight moving parallel to itself through a stationary turbulence configuration with speed v.*

$$W(f) = \frac{8\pi^3 \left\langle \Delta N^2 \right\rangle 10^{-12} \ell_o^2 L}{\lambda^2 v} \cdot \frac{1}{\left[1 + \left(\frac{2\pi f \ell_o}{v}\right)^2\right]^{3/2}} \qquad (2.55)$$

One may identify v with a local wind speed, which blows the (stable) turbulence structure through the line-of-sight. This expression is halved when $f = 0.122\, v/\ell_o$, so that with v = 20 ft./sec and ℓ_o = 100 feet, an effective (noise) bandwidth B = 0.02 cps is produced. Very near the ground, one has ℓ_o = 10 feet, so that $B \simeq 0.2$ cps.

The received power is also smeared over a small solid angle centered on the line-of-sight. Off-axis turbulent clusters scatter energy into the antenna according to the angular distribution, Eq. (2.13). This ratio is reduced by a factor of four when θ becomes $\frac{\lambda}{2\pi\ell_o} \simeq \frac{1}{3} 10^{-3}$ radians, which represents a very narrow pencil of rays indeed.

We have also investigated the angle-of-arrival fluctuations which the direct ray experiences. The exponential correlation, Eq. (2.2) produces an infinite RMS deviation because of its cusp-like behavior at the origin. In general, the spectrum widths for deviation of the rays is of the same order of magnitude as that for the phase variations. It would be of great interest to

---

* $\int_{-\infty}^{\infty} df\, W(f) = \left\langle a^2 \right\rangle_{direct}$.

repeat the foregoing calculations when a better correlation function is established on physical grounds.

III. RAINFALL

The theory of multipath transmission through singly scattering media developed in Part II may be exploited to discuss rain-produced scintillation errors as a radar beam traverses a precipitation area. The drops will be idealized as perfect dielectric spheres. The entire signal perturbation thus results from classical scattering and no phase disturbance of the direct wave is considered. When these results are combined with appropriate meteorological data, the theory predicts both angular distributions and phase error frequency spectra for the received power.

A. Static Multipath Effects

Our description begins with an expression for the scattering by a single droplet, as illustrated in Fig. 9. Since the raindrops are considered spherical, one must deduce the ratio of scattered-to-incident power for a sphere of radius a and dielectric constant ϵ. This quantity has been computed by classical electromagnetic theory in many places.[19][20] We shall see presently that most raindrops are less than 2 millimeters in diameter, and, since we consider microwave propagation, one may pass directly to the Rayleigh limit ($2\pi a/\lambda \ll 1$),

---

[19] D. E. Kerr, Propagation of Short Radio Waves, MIT Rad. Lab. Series, New York, McGraw-Hill, 13, 445 (1951).

[20] J. A. Stratton, Electromagnetic Theory, New York, McGraw-Hill, p. 563 (1941).

$$\frac{S(R)}{Sinc.} = \frac{\lambda^2}{4\pi^2 \cdot R^2} \left|\frac{\epsilon - 1}{\epsilon + 2}\right|^2 \left(\frac{2\pi a}{\lambda}\right)^4 \left[\sin^2(\phi) + \cos^2(\theta)\cos^2(\phi)\right], \tag{3.1}$$

representing reradiation by the drop as an electric dipole. The scattering cross section per droplet per unit solid angle is obtained by multiplying this ratio by $4\pi R^2$. To compute the scattering cross section per unit volume, which appears in the multipath density Eq. (2.8), one must estimate the number of drops per unit volume in each radius interval (da). Rigby and Marshall have fitted the exponential function Eq. (3.2) to meteorological experiments.[21]

$$\frac{dN}{dadv} = c \cdot \exp -\left[\frac{2a}{b}\right] \frac{drops}{(cm)(cm^3)} \tag{3.2}$$

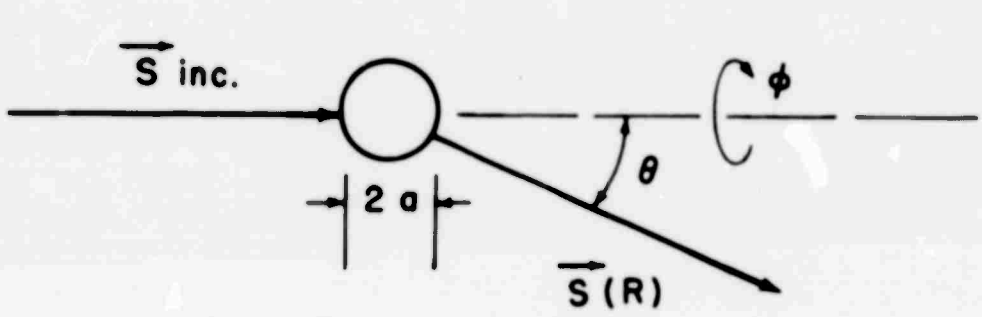

Figure 9

Scattering of a Plane Wave by a Spherical Drop

Their normalization constant c is roughly 0.08 and the "drop scale size parameter," b, is given in terms of the rainfall rate R (measured in millimeters per hour), by

(21) E. C. Rigby and J. S. Marshall, "Modification of Rain with Distance Fallen," Scientific Rpt. MW-3, MacDonald Phys. Lab., McGill University, Jan. 1952.

$$b = \frac{R^{0.21}}{41} \text{ (cm)} \ . \qquad (3.3)$$

Table I correlates R and b with familiar precipitation intensities.

Table I

Rainfall Rate Versus Drop Scale Size

Rain Type	R	b
Drizzle	0.25 mm/hour	0.018 cm
Light Rain	1.00 "	0.024 "
Moderate Rain	4.00 "	0.033 "
Heavy Rain	10.00 "	0.040 "
Very Heavy Rain	16.00 "	0.044 "
"	20.00 "	0.046 "
"	25.00 "	0.048 "
"	30.00 "	0.050 "
"	50.00 "	0.055 "
"	100.00 "	0.064 "
"	150.00 "	0.070 "

Expression (2.8) for the static multipath power distribution may now be computed by combining Eq. (3.1) and (3.2) and averaging over all drop sizes.

$$\frac{Q(x)}{P_o} = \int_o^\infty da\ c\ e^{-2a/b} \int' dr \int' d\theta \sin\theta \int_o^{2\pi} d\phi\ 4\pi a^2 \left|\frac{\epsilon - 1}{\epsilon + 2}\right|^2 \left(\frac{2\pi a}{\lambda}\right)^4$$

$$\cdot \left[\sin^2(\phi) + \cos^2(\theta)\cos^2(\phi)\right] \cdot \delta\left[x - r(1 - \cos\theta)\right] \ . \qquad (3.4)$$

A spherical coordinate system erected on the receiver's pointing direction has been used to write out the beam-limited (primed) volume integral (see Figure 10). For a narrow beam, one may disregard the entrance disparities between

extreme rays of the multipath reception cone which is tantamount to restricting the radial integral by $R_1 \text{ Sec}(\theta) < r < R_2 \text{ Sec}(\theta)$.

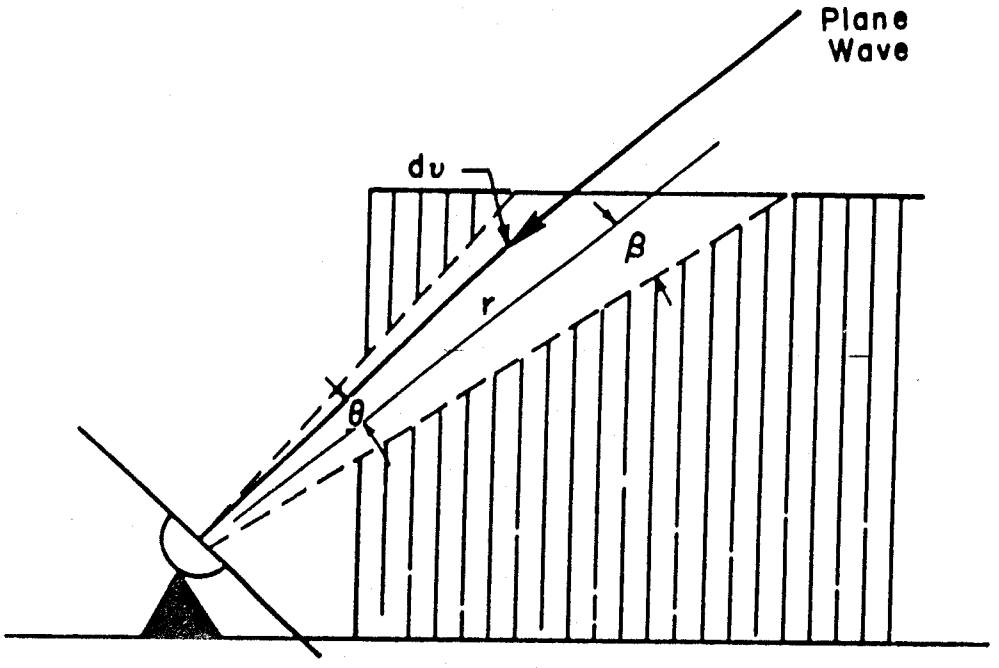

Figure 10
Coordinates for Scattering by Rainfall

(1) Phase Delay

With Eq. (3.4) and the superposition of Figure 3, one computes the RMS phase error in a sinusoidal voltage received at the origin as:

$$\langle a^2 \rangle = \int_0^\infty dx \sin^2\left(\frac{2\pi x}{\lambda}\right)^4 \cdot \frac{Q(x)}{P_o} ,$$

$$\simeq 9 b^3 \left(\frac{2\pi b}{\lambda}\right)^4 \int_0^\beta d\theta \sin\theta \left[1 + \cos^2(\theta)\right] \cdot \left|\frac{\epsilon - 1}{\epsilon + 2}\right|^2$$

(continued on following page)

$$\left\{ \frac{R_2 - R_1}{\cos(\theta)} - \frac{\sin\left[\frac{4\pi R_2}{\lambda}(\mathrm{Sec}\,\theta - 1)\right]}{4\pi/\lambda} + \frac{\sin\left[\frac{4\pi R_1}{\lambda}(\mathrm{Sec}\,\theta - 1)\right]}{4\pi/\lambda} \right\} . \qquad (3.5)$$

The trigonometric terms may be ignored in comparison with the viewing thickness $(R_2 - R_1)$; and the dielectric constant (ϵ) assumed constant to our approximation.

$$\langle a^2 \rangle \simeq 9 b^3 \left(\frac{2\pi b}{\lambda}\right)^4 \left|\frac{\epsilon - 1}{\epsilon - 2}\right|^2 \cdot (R_2 - R_1)\, \mathcal{J}(\beta) . \qquad (3.6)$$

$\mathcal{J}$ denotes a beam shape factor,

$$\mathcal{J}(\beta) = \int_0^\beta \frac{d\theta \sin(\theta)}{\cos(\theta)} \left[1 + \cos^2(\theta)\right] ,$$

$$\simeq \beta^2 \qquad \text{for} \qquad \beta << 1 . \qquad (3.7)$$

Our result indicates that $\langle a^2 \rangle$ varies about as the seven-tenths power of the rainfall rate and directly with the square root of the total number of participating droplets. This latter dependence is characteristic of incoherent scattering processes and might have been anticipated from the original assumptions. To provide numerical estimates for Eq. (3.6), we note that the dielectric constant of water varies from $\epsilon = 78.5 - i\,12.3$ at $\lambda = 10$ cm to $34.2 - i\,35.9$ at $\lambda = 1.24$ cm for $t = 18^\circ C$.[19] The corresponding values of $\left|\frac{\epsilon - 1}{\epsilon + 2}\right|^2$ range from 0.9286 to .9206, and we shall choose the average value 0.925. In Figure 11, we plot $\langle a^2 \rangle / \mathcal{J} \cdot (R_2 - R_1)$ for various wavelengths (λ) and rainfall rates (R). From those curves we read for $\lambda = 6$ cm and R = 100 mm/hour (i.e., a very heavy rain),

[19] D. E. Kerr, op. cit., page 610.

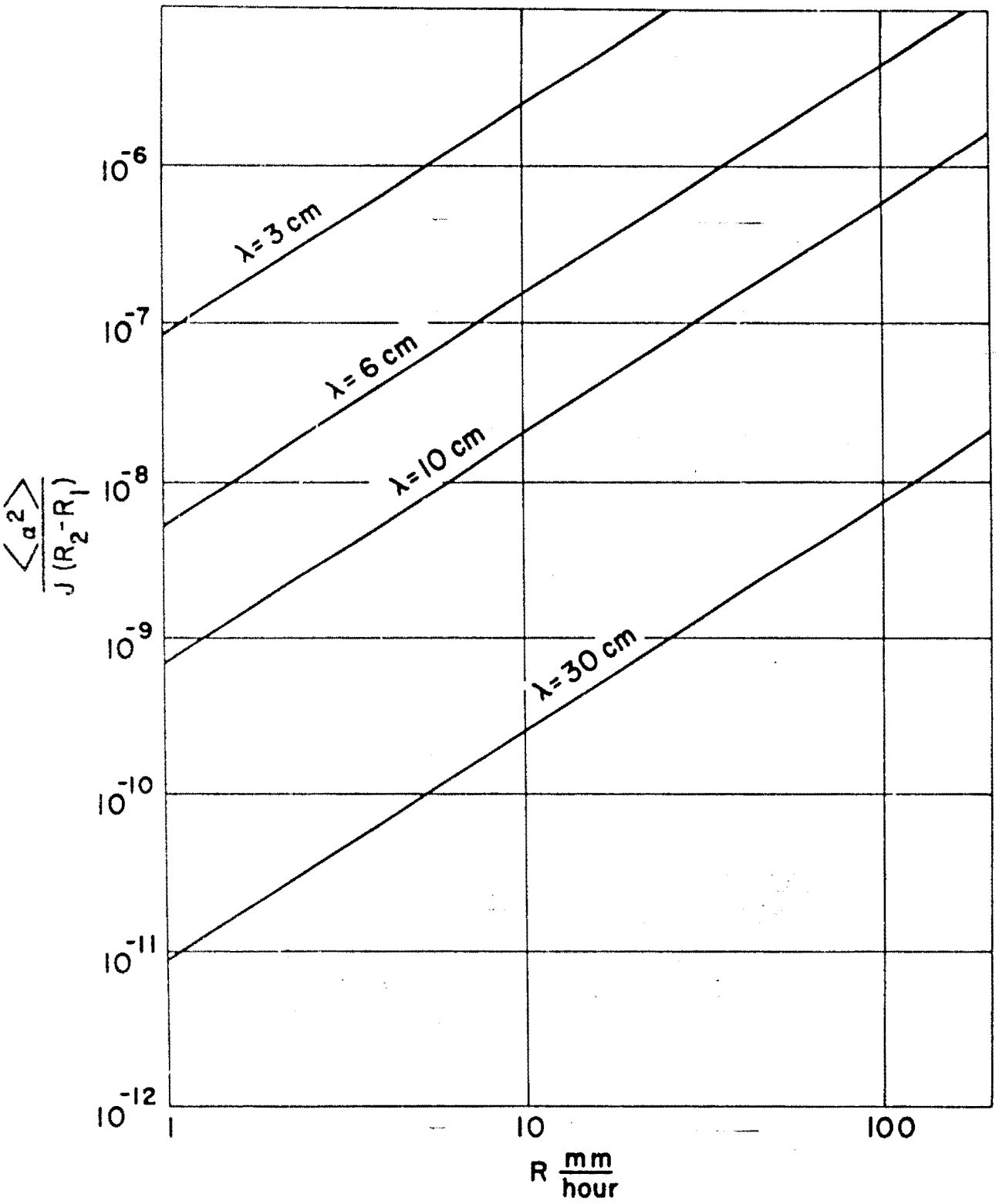

Figure 11

RMS Phase Error for Scattering by Rainfall

$$\langle a^2 \rangle \simeq 4.5 \cdot 10^{-6} (m^{-1}) \beta^2 (R_2 - R_1) . \qquad (3.8)$$

A typical antenna beam $\beta = 4^o$ and rainstorm, $R_2 - R_1 = 1000$ meters predicts,

$$a_{RMS} \simeq 1.75 \cdot 10^{-2} \text{ radians} . \qquad (3.8a)$$

This error is an order of magnitude larger than the scattering effect of static tropospheric turbulence derived in Part II. The sensitivity of Eq. (3.6) to $(R_2 - R_1)$ and the rainfall rate (R) encourage one to estimate local meteorological conditions with some care before attempting precision measurements.

(2) Angular Distribution

An angular distribution of power about the receiving antenna's pointing direction is predicted by the foregoing theory. If one integrates expression (3.4) over all path differences (x), the total scattered power becomes:

$$\frac{P_s}{P_o} = \int_o^{\beta} d\theta \sin(\theta) \int_o^{\infty} da\, c\, e^{-2a/b} \int_{R_1 \mathrm{Sec}\,\theta}^{R_2 \mathrm{Sec}\,\theta} dr \int_o^{2\pi} d\phi\, 4\pi a^2 \left| \frac{e - 1}{e + 2} \right|^2$$

$$\cdot \left(\frac{2\pi a}{\lambda} \right)^4 \left[\sin^2(\phi) + \cos^2(\theta) \cos^2(\phi) \right] . \qquad (3.9)$$

The angular dependence of this scattered power is recognized as the integrand of the cos(θ) integration.

$$\frac{1}{P_o} \frac{dP_s}{d(\cos\theta)} = \frac{4\pi^2 (6)!}{2^7} c \left(\frac{2\pi b}{\lambda} \right)^3 \cdot b^3 (R_2 - R_1) \left[\frac{1 + \cos^2(\theta)}{\cos(\theta)} \right] \qquad (3.10)$$

The angle-dependent factor is plotted in Figure 12, where a relatively flat distribution for small beamwidths is exhibited. Increasing values of this function for large θ are due to the inclusion of an ever-increasing number of

scatterers—the number going to infinity as near horizontal viewing is included. A realistic consideration of attenuation effects rectifies this problem. We shall continue to use the natural cut-off of narrow beam antennae.

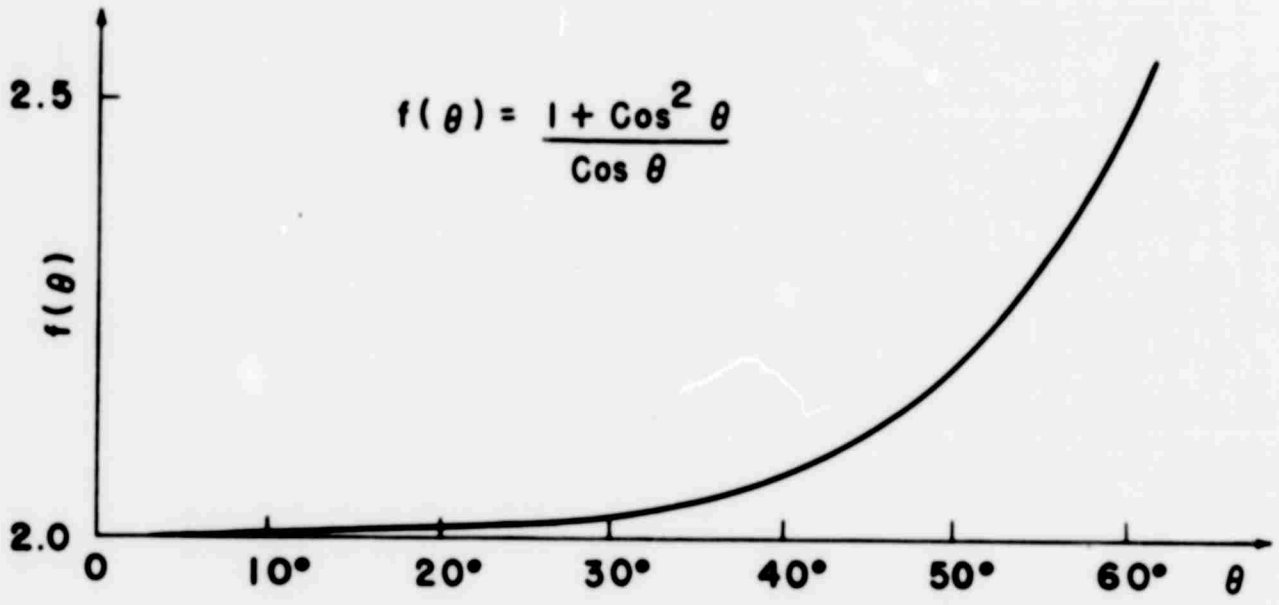

Figure 12
Angular Distribution of Rainfall-Scattered Power

B. Scintillation Spectra

In the foregoing we derived an expression for the RMS value of the multipath phase error. Of equal importance is the frequency spectrum of the phase scintillations. The anomolous signal is compounded from the scatterings by thousands of raindrops in the beam. Time variations of the phase error may be regarded as the composition of Doppler frequency shifts from the individual droplets moving relative to one another in changing order. We may anticipate the magnitude of these frequencies from the Doppler relation:

$\Delta f = u/c\, f_o$. For relative drop speeds of one meter per second and $f_o = 5000$ mcs, $\Delta f = 16$ cps and such a scintillation is evidently of some importance in precision measurements.

We first resolve all drop velocities along the pointing (z) direction of the antenna, as shown in Figure 12. If the incident plane wave meets a drop at dv with speed u, the drop's motion away from the incident wave lowers the incident frequency (seen by the moving drop) by an amount $u/c\, f_o$. The drop reradiates this shifted frequency at an angle θ to the incident beam thereby causing an increase $f_o\, u/c \cos(\theta)$. The net frequency change during the scattering process is $\Delta f = f_o \cdot u/c \cdot (1 - \cos\theta)$. We shall construct a joint path difference-frequency power spectrum for the multipath signal scattered by the volume element dv at (r, θ, ϕ) moving with speed u parallel to the incident beam. By using the analytical device introduced in Eq. (2.6) of Part II, one may show that the ratio of the scattered-to-incident power with path difference between x and x + dx and signal frequency between f and f + df is given by:

$$\frac{Q(x,f)}{P_o} = \int_o^\infty da\, N(a) \int_o^\infty du\, P(u|a) \int' \frac{dv}{r^2}\, \sigma_i(a; r, \theta)\, \delta\left[x - r(1 - \cos\theta)\right]$$

$$\cdot\, \delta\left[f - f_o - f_o \frac{u}{c}(1 - \cos\theta)\right]. \qquad (3.11)$$

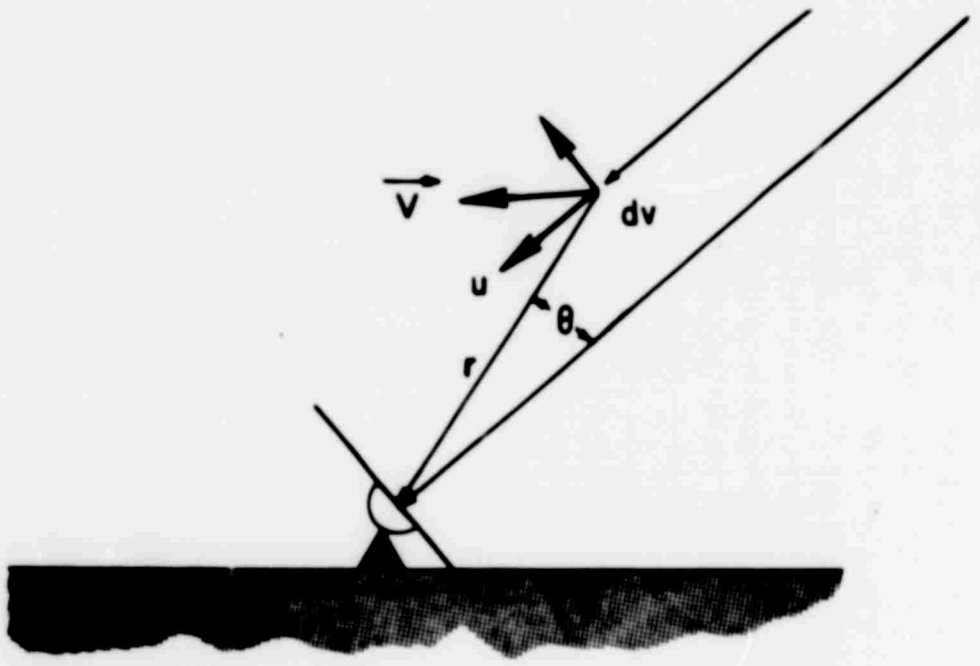

Figure 13
Drop Velocity Resolution for Doppler Shift Analysis

A prime on the volume integration restricts that process to the radar beam. P(u|a) denotes the conditional probability distribution for a velocity component u parallel to the antenna axis for drops with radius a. We do not know this density a priori, and its determination is the central problem of this section. We shall see presently how one may infer P(u|a) from other propagation experiments—notably, backscattered (echo) fluctuations from rainfall.

The integrations of Eq. (2. 54) may be performed with relative ease if one assumes P(u|a) to be independent of drop size (a). Such an assumption is probably warranted if the relative drop motion is due to local gusts and turbulent conditions in the rainfall area.* In a C. W. phase comparison system, the scintillation frequencies are given by excursions from the carrier frequency

*It is also possible to obtain a Doppler shift from the differential speeds with which drops of different sizes fall. This effect can be calculated from Stoke's law for the fall of spheres in a viscous medium. We shall return to this case later for comparison.

f_o, so that the frequency spectrum is a function of $\nu = f - f_o$. Inserting the appropriate forms for N(a) and σ from Eq. (3.2) and Eq. (3.1) respectively, one finds:

$$\frac{Q(x,\nu)}{P_o} = \int_o^\infty du\, P(u) \int_o^\infty da\, c\, e^{-2a/b} \int_o^\beta d\theta \sin(\theta) \int_{R_1}^{R_2} dr \int_o^{2\pi} d\phi$$

$$\cdot \left\{ 4\pi a^2 \left| \frac{\epsilon - 1}{\epsilon + 2} \right|^2 \left(\frac{2\pi a}{\lambda} \right)^4 (\sin^2(\phi) + \cos^2(\phi) \cos^2(\theta)) \right\}$$

$$\cdot \delta\left[x - r(1 - \cos\theta) \right] \cdot \delta \left[\nu - f_o \frac{u}{c} (1 - \cos(\theta) \right] . \qquad (3.12)$$

(1) Phase Delay

If one uses this expression to compute the phase error, the frequency spectra for a^2 emerges without further effort.

$$\langle a^2(\nu) \rangle = \int_o^\infty dx \sin^2 \left(\frac{2\pi x}{\lambda} \right) \frac{Q(x,\nu)}{P}$$

$$= \frac{\pi}{2} (R_2 - R_1) g(\lambda) \frac{c}{f_o} \int_o^\beta d\theta \frac{\sin(\theta)}{1 - \cos(\theta)} \left[1 + \cos^2(\theta) \right]$$

$$\cdot P \left[\frac{c \cdot \nu}{f_o (1 - \cos(\theta)} \right] . \qquad (3.13)$$

The frequency dependence of the forward scattering is apparent from Eq. (3.13). Since the velocity distribution's argument $c/f(1 - \cos\theta)^{-1}$ is large for the small values of $(1 - \cos\theta)$ inherent in a narrow beam, the net effect is to relegate most of the scintillation power to small frequencies. $g(\lambda)$ denotes a wave length-dependent term arising from the drop radius averaged cross section.

$$g(\lambda) = \int_0^\infty da\,(c\,\epsilon^{-2a/b})\,4\pi a^2 \quad \left|\frac{\epsilon - 1}{\epsilon + 2}\right|^2 \quad \left(\frac{2\pi a}{\lambda}\right)^4$$

$$= 0.08\,4\pi b^3 \quad \left(\frac{2\pi b}{\lambda}\right)^4 \left|\frac{\epsilon - 1}{\epsilon + 2}\right|^2 \cdot \frac{(6)!}{2^7}$$

$$- \frac{1}{2} b^3 \quad \left(\frac{2\pi b}{\lambda}\right)^4 . \qquad (3.14)$$

We assume $\left|\frac{\epsilon - 1}{\epsilon + 2}\right|^2 \simeq 0.925$, as before, and b is given in terms of the rainfall rate R by Eq. (3.3).

To determine the function P(z), we shall first exploit experimental data on spectral analysis of precipitation echoes.

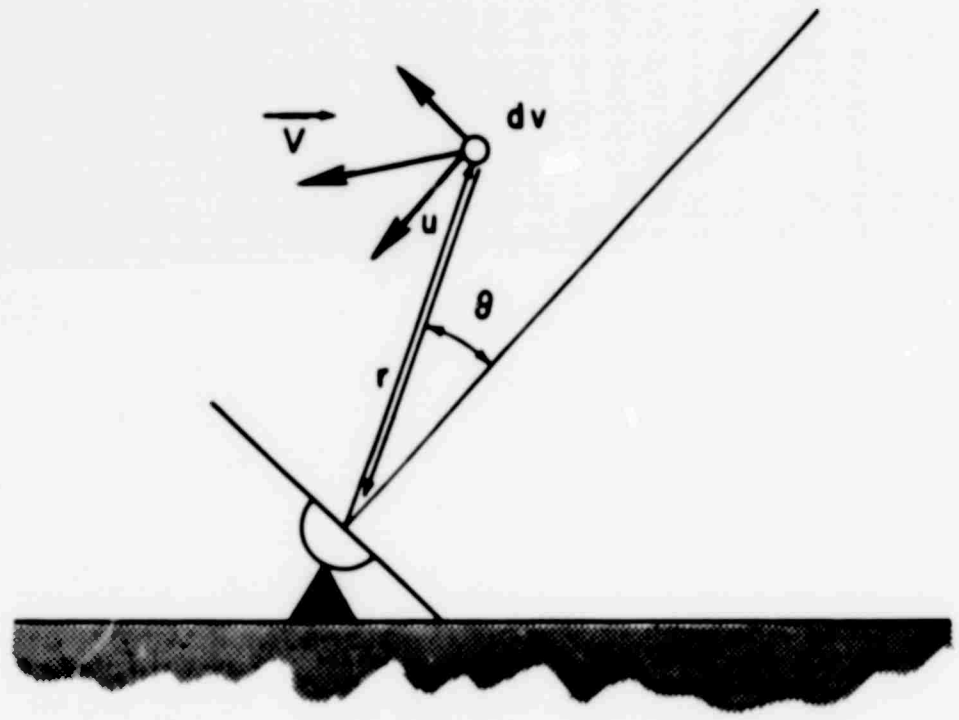

Figure 14
Echo Process for Moving Drops

Figure 14 exhibits the backscattering process for a moving drop. A plane wave sent out by the antenna θ radians off-axis enjoys a frequency shift $u/c \cos\theta$, both on reception and reradiation. The appropriate variation of Eq. (3.11) for the backscattered amplitudes is

$$\frac{R(x,\nu)}{P_o} = \int_o^\infty da\, N(a) \int_o^\infty du\, P(u|a) \int' \frac{dv}{r^2}\, \sigma_{B.Sc.}(a)$$

$$\cdot\, \delta\left[x - r(1 - \cos\theta)\right] \cdot \delta\left[\nu - 2f_o \frac{u}{c} \cos\theta\right] . \qquad (3.15)$$

An amplitude scintillation spectrum may be deduced from this form by integrating over (x) and substituting the appropriate backscattering cross section from Eq. (3.1).

$$\left\langle B^2(\nu)\right\rangle = P_o \int_o^\infty da\, N(a)\, 4\pi a^2 \left|\frac{\epsilon - 1}{\epsilon + 2}\right|^2 \cdot \left(\frac{2\pi a}{\lambda}\right)^4 \int_o^\infty du\, P(u)$$

$$\cdot \int_o^\beta d\theta \sin(\theta) \int_{R_1}^{R_2} dr \int_o^{2\pi} d\phi \int_o^\infty dx\, \delta\left[x - r(1 - \cos\theta)\right]$$

$$\cdot\, \delta\left[\nu - 2f_o \frac{u}{c} \cos(\theta)\right]$$

$$= P_o g(\lambda)\pi(R_2 - R_1) \frac{c}{f_o} \int_o^\beta d\theta \tan(\theta)\; P\left[\frac{c\,\nu}{2f_o \cos(\theta)}\right] . \qquad (3.16)$$

The spectrum normalized to unity at $\nu = 0$ is simply,

$$G(\nu) = \frac{\int_o^\beta d\theta \tan(\theta)\, P\left[\frac{c\,\nu}{2f_o \cos(\theta)}\right]}{P(o)\, \ell n\left[\cos(\beta)\right]} . \qquad (3.16')$$

The small ($<4^o$) values assumed for β permit one to replace $\cos\theta$ by unity in Eq. (2.61) and thus extract $P(z)$ from within the integrand.

$$P\left[\frac{c}{2f_o}\right] \approx P[o]\, G(\nu) \,. \qquad (3.17)$$

This important relation permits one to infer the velocity distribution of raindrops from the experimental* echo fluctuation spectra $G(\nu)$. In Figure 15 we reproduce the measurements of Goldstein and others[19] for $\lambda = 9.2$ cm, as measured on three occasions. These curves give just the normalized (Doppler) frequency power density of the backscattered amplitudes, $G(\nu)$.

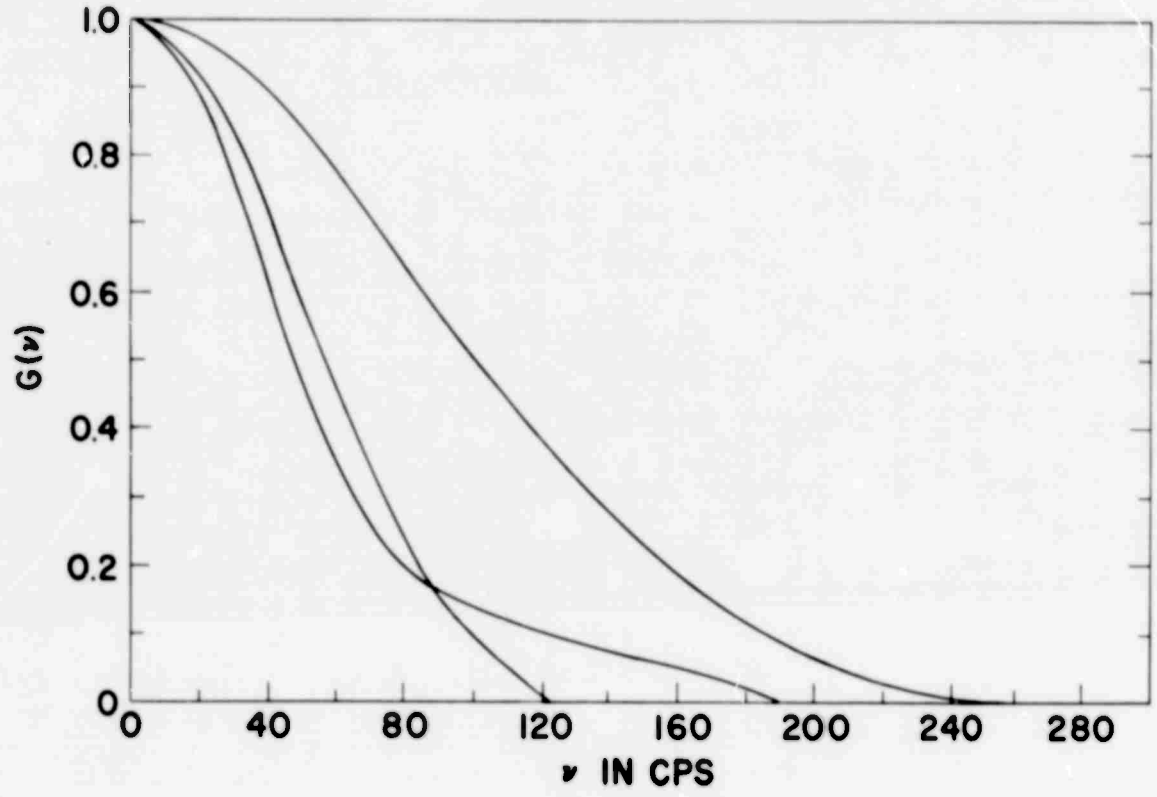

Figure 15

Power Frequency Spectrum of the Fluctuations of
Precipitation Echo on 9.2 cm as Measured on Three Occasions

*Note that Eq. (3.17) is independent of the beamwidth (β) used in these experiments.

[19] D. E. Kerr, op. cit., page 576.

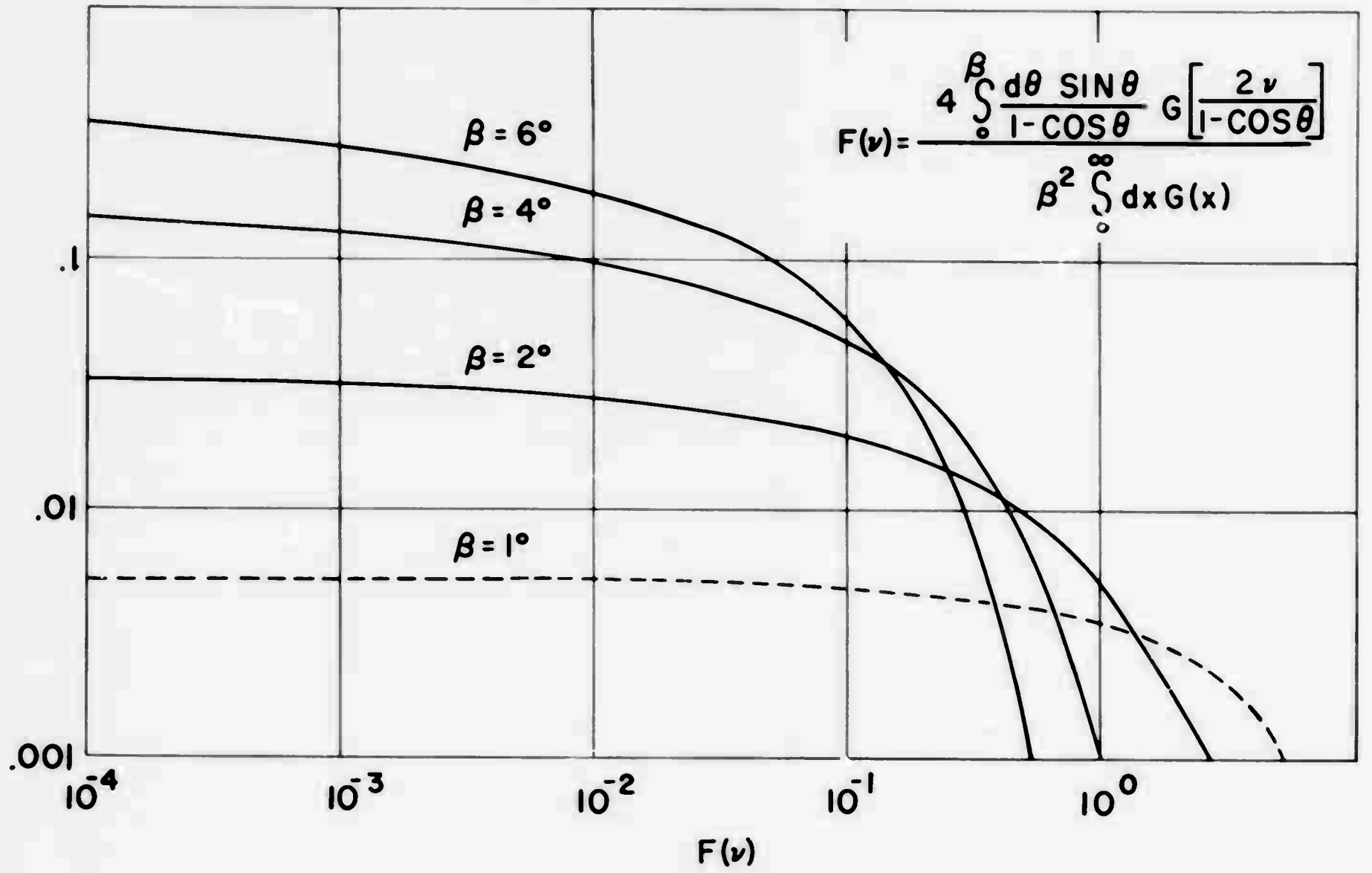

Figure 16
Phase Error Spectra for Rainfall Scattering

Our integral expression (3.13) for the phase error may now be combined with Eqs. (3.16') and (3.17) to yield:

$$\left\langle a^2(\nu) \right\rangle = \frac{\pi}{2}(R_2 - R_1)g(\lambda) \cdot \frac{c}{f_o} P(o) \int_o^\beta \frac{d\theta \sin(\theta)}{1 - \cos(\theta)}$$

$$\cdot \left[1 + \cos^2(\theta)\right] \cdot G\left[\frac{2\nu}{1 - \cos(\theta)}\right] . \qquad (3.18)$$

The remaining integration has been performed numerically using the values for $G(\nu)$ given by Figure 15. In Figure 16, we plot the normalized* spectrum for several beamwidths (β). These curves emphasize the concentration of power at low frequencies.

One may also compute a phase angle spectrum by considering the detailed motion of individual drops. Imagine an ensemble of drops falling through stagnant air under gravity. The viscous drag force predicts greater fall speeds for heavy drops than for light ones. Extremely small spheres ($a < 0.008$ cm) obey Stoke's law for steady state terminal velocity,**

$$v^2 = \frac{8}{3} g a \left[\frac{\rho_s}{\rho_a} - 1\right] \cdot \frac{1}{C_D}$$

Very large drops are relatively unstable and tend to break up into smaller ones during long descents. The intermediate region is of some interest for this study, in view of the drop scale sizes listed in Table I. Fortunately enough,

---

*Normalized so that $\int_o^\infty d\nu \left\langle a^2(\nu) \right\rangle = 1$.

**C_D denotes the drag coefficient, ρ_a the air density, ρ_s the drop density; a is the drop radius and g the acceleration of gravity.

Gunn and Kinzer[22] have measured the terminal velocities of drops with diameters in the range $0.01 < D < 0.68$ cm. Their results may be summarized by an approximate formula,

$$v(a) = K\left[1 - e^{-\Lambda a}\right] \tag{3.19}$$

with $K = 1020$ m/sec and $\Lambda = 5.04\ \text{cm}^{-1}$. The conditional probability density $P(u|a)$ for the distribution of velocities with fixed radius (a) may be given explicit form in terms of Eq. (2.19).

$$P(u|a) = \delta\left[\vec{u} - \vec{K} \cdot v(a)\right] . \tag{3.20}$$

If the angle between the local vertical (i.e., $\vec{k}$) and the antenna's pointing direction is denoted by γ, then $u = v\cos(\gamma)$. Equations (3.13), (3.19), and (3.20) may then be combined to give the phase angle spectrum:

$$\langle a^2(\nu)\rangle = \int_0^\infty dx \sin^2\left(\frac{2\pi x}{\lambda}\right)\int_0^\infty daN(a)\int_0^\infty du\,\delta\left[u\sec(\gamma) - v(a)\right]$$

$$\cdot \int_0^\beta d\theta \sin(\theta)\int_{R_1}^{R_2} dr \int_0^{2\pi} d\phi\,\sigma(\theta,\phi;a)\,\delta\left[x - r(1-\cos\theta)\right]$$

$$\cdot\ \delta\left[\nu - f_o\frac{u}{c}(1-\cos\theta)\right]$$

$$\simeq 4\pi^2(0.08)(R_2 - R_1)\frac{c}{f_o}\cdot\left|\frac{e-1}{e+2}\right|^2\int_0^\infty da\,a^2$$

$$\cdot\left(\frac{2\pi a}{\lambda}\right)^4\cdot\frac{e^{-(2a/b)}}{v(a)} .$$

[22] R. Gunn and G. D. Kinzer, Jour. of Meteorology, 6, 243 (1949). Their experiments were performed under 760 mm pressure, with a temperature of 20°C and relative humidity of 50 per cent.

The scintillation frequency (ν) persists in the (drop-size) integration condition,

$$v(a) > \frac{c\nu}{f_o} \frac{\sec(\gamma)}{1 - \cos(\beta)} . \tag{3.23}$$

If the curve-fitted function (3.19) is inserted, the (origin-normalized) phase spectrum becomes:

$$F(\nu) = \frac{\int_{\zeta}^{\infty} da \frac{a^6 e^{-(2a/b)}}{1 - e^{-\Lambda a}}}{\int_{0}^{\infty} da \frac{a^6 e^{-(2a/b)}}{1 - e^{-\Lambda a}}}, \tag{3.24}$$

with

$$\zeta = \frac{1}{\Lambda} \ln\left[1 - \frac{\nu c}{K f_o} \cdot \frac{\sec(\gamma)}{(1 - \cos\beta)}\right]. \tag{3.24'}$$

It is clear from this form that all frequencies greater than

$$\nu_{max} = \frac{K}{c} f_o \cos(\gamma)(1 - \cos\beta)$$

are eliminated in Eq. (3.24). We may estimate this cut-off by assuming: $f_o = 5000$ mcs, $\cos\gamma = 0.4$, $\beta = 4^o$, $K = 10^3$ m/sec, so that $\nu_{max} = 16$ cps. The quotient (3.24) was computed numerically for moderately heavy rain, R = 4 mm/hour and is displayed in Figure 17 for the range $0.01 < \nu < 16$ cps.

Rather less realism may be associated with this model than the radar-precipitation echo approach. This statement is based on the common experience that heavy rainstorms are fraught with turbulent gusts, each probably sufficient to dominate the laboratory result (4.19). It would be very valuable, however, to perform a controlled experiment measuring line-of-sight

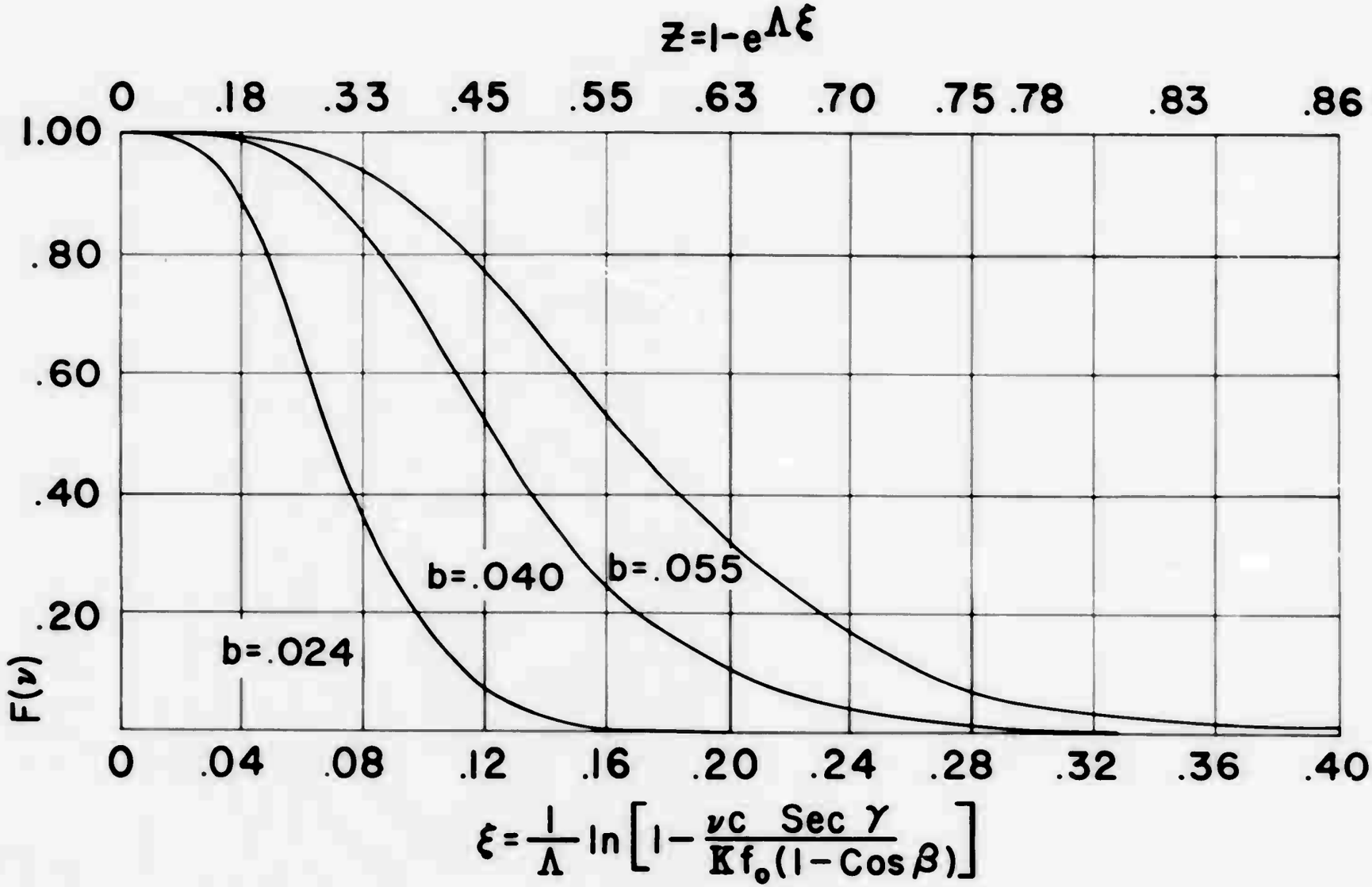

Figure 17

Phase Error Spectrum for Scattering by Falling Drops

and echo scintillations simultaneously within the same rainstorm. Such a test could criticize the result (3.16') and perhaps give information on the mixture of turbulent and free-fall drop motion within rainstorms.

C. Ray Bending in Rainstorms

In addition to scattering off-axis energy into the antenna, a rainstorm will act as a prism and bend rays passing completely through it. If the drop sizes are small compared with the wavelength of the incident radiation, the equivalent index of refraction for a collection of perfect dielectric spheres $\left[|\epsilon| \gg 1\right]$ is:

$$\eta = 1 + 2\pi a^3 N \, . \tag{3.25}$$

Here a is the sphere radius and N the number of spheres per unit volume. One may use Eq. (3.2) to average this expression over all drop sizes.

$$\langle \eta \rangle \simeq 1 + 0.2 b^4 \tag{3.26}$$

For a heavy rain R = 10 mm/hour , b = 0.04 and

$$\langle \eta \rangle \simeq 1 + \frac{1}{2} \cdot 10^{-6} \, . \tag{3.27}$$

The bending at entrance and exit of a ray passing through such a region can be computed with standard techniques.

When the drop spacing is small compared with the wavelength, one must exploit a detailed picture of the scattering processes. H.C. Corben[23] has performed such an analysis and concludes that the essential factors in Eq. (3.25) are preserved. He finds that multiple scattering may be disregarded for most applications.

---

[23] Private communication, August, 1954.

IV. CLOUDS

Index of refraction data for clouds are notably sparse. From meteorological measurements and aircraft gust load experience. However, it is known that the interiors of cloud formations are very turbulent and contain relatively large index fluctuations. Extensive circulation and mixing is known to take place within clouds, in addition to over-all movement and structural rearrangements.[24][25] Both directional and turbulent currents of very dense water vapor suggest a "tighter" correlation than that found in free air. Records of refractometer flights[26][27] through clouds substantiate this, and indicate that the scale of turbulence is probably of the order 10 to 20 feet. These same records suggest that RMS excursions of the index of refraction may be as large as 10 or 20 N units. Such results characterize a turbulent medium far more active and influential for microwave frequencies than was considered in Part II. We shall therefore undertake a separate determination of propagation through cloud structures.

---

[24] J. S. Malkus and C. Ronne, Wood's Hole Oceanographic Institution, Ref. No. 54-18, March, 1954.

[25] J. S. Malkus and R. S. Scorer, Wood's Hole Oceanographic Institution, Ref. No. 54-5, January, 1954.

[26] C. M. Crain, A. P. Deam, and J. R. Gerhardt, Proc. I.R.E., 41, 253 (1953).

[27] G. Birnbaum and H. Bussey, Journal of Research, 51, 171 (1953).

A. Cloud Scattering

We may estimate the effect of (uniform) turbulence scattering in a cloud layer* of thickness L with the results developed in Part II. Consider a cloud at mean distance R from the receiver as shown in Figure 18. Expression (2.11) yields:

$$\left\langle a^2 \right\rangle \simeq \int_0^\infty dx \sin^2\left(\frac{2\pi x}{\lambda}\right) \int_R^{R+L} dr \int_0^\beta d\theta \sin(\theta) \int_0^{2\pi} d\phi\, \sigma(\theta,\phi) \cdot \delta\left[x - r\,(1 - \cos\theta)\right],$$

$$\simeq \left(\frac{2\pi\, o}{\lambda}\right)^3 \cdot \left\langle \Delta N^2 \right\rangle 10^{-12} \int_0^U du \, \frac{\left[1 - \frac{\sin u}{u}\right]}{\left[1 + \frac{2\pi \ell_o^2}{\lambda H} \cdot u\right]^2} , \qquad (4.1)$$

with

$$U = \frac{4\pi H}{\ell_o}\left[1 - \cos\beta\right] .$$

We shall return to a numerical evaluation of this expression for the relevant cloud turbulence parameters in Part C.

B. Direct Wave in Clouds

(1) Phase Variation

We shall exploit the general method of Section II B to calculate the phase shi. n the direct ray due to turbulence within a cloud. It will be assumed that the turbulence pattern within the cloud is stationary with respect

*Layer scattering has also been considered in connection with beyond-line-of sight propagation[28] and the scintillation of galactic radio waves.[29]

[28] W. E. Gordon, Proc. Conference on Radio Meteorology, Univ. of Texas, November, 1953.

[29] E.C.S. Megaw, Nature, 166, 1100.

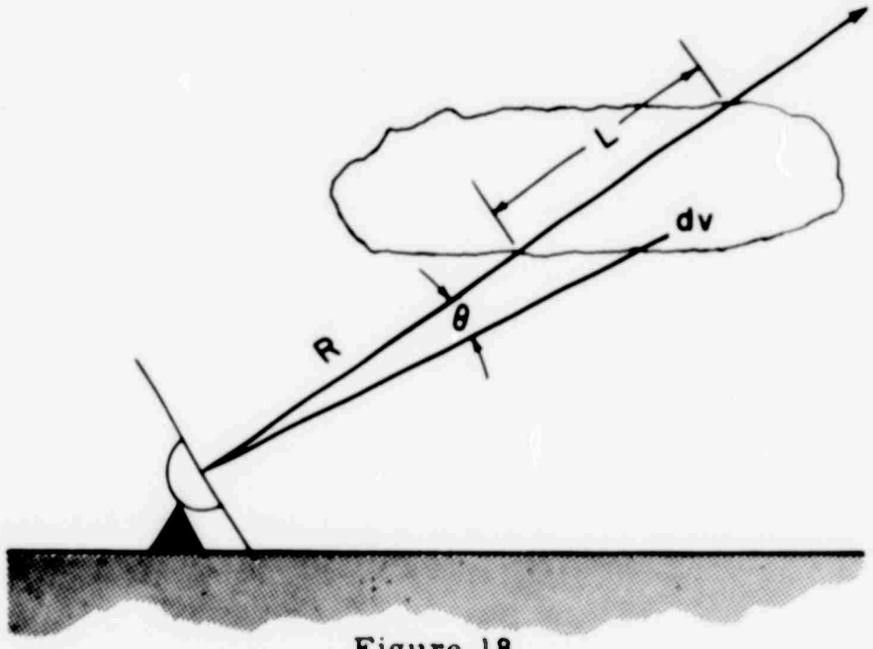

Figure 18

Scattering by Cloud Layer

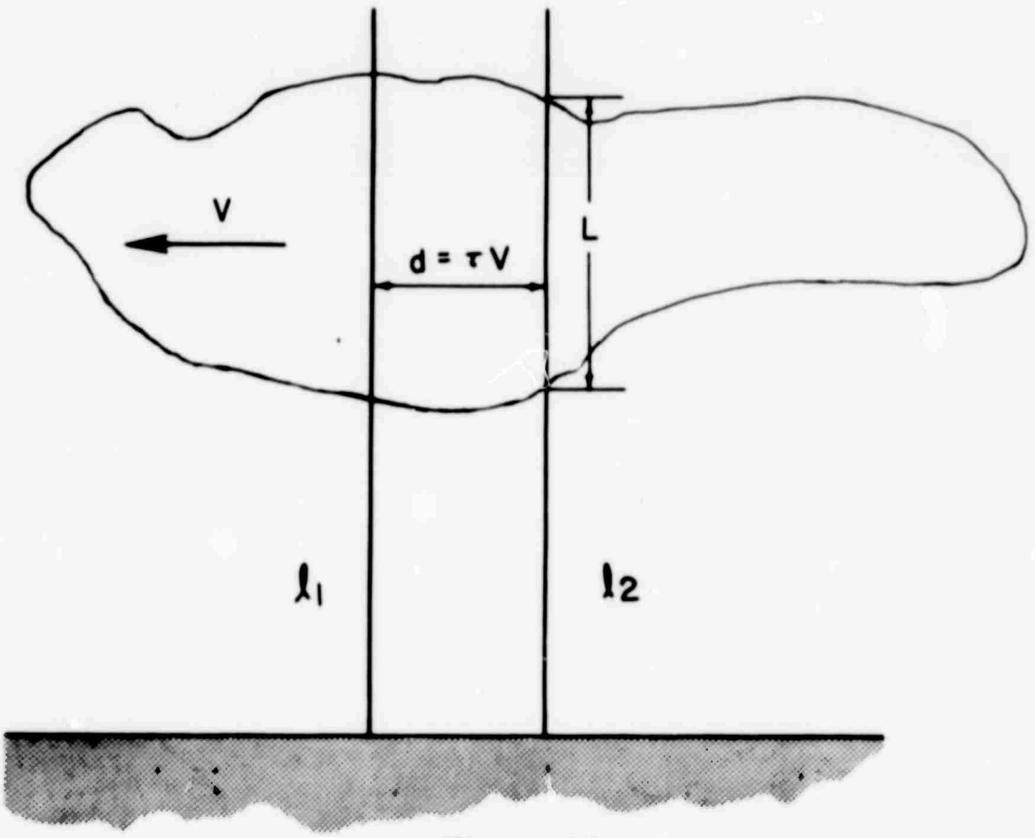

Figure 19

Geometry for Line-of-Sight Moving Parallel to Itself

to the cloud. The line-of-sight sweeps through this pattern, either because of the cloud's over all motion or due to an actual translation of the propagation path. The initial line-of-sight is denoted by ℓ_1, and τ seconds later by ℓ_2. The space interval between the two points ℓ_1 and ℓ_2 is $d = v\tau$ where v is the velocity of the cloud and/or path (see Figure 19).

The autocorrelation of the phase shift is computed as in Eq. (2.20), with the correlation (space) interval defined by:

$$r_{12} = \sqrt{(\ell_2 - \ell_1)^2 + (v\tau)^2} \quad . \tag{4.2}$$

Therefore:

$$\langle a(t)a(t+\tau)\rangle = \frac{4\pi^2 10^{-12}\langle \Delta N^2\rangle}{\lambda^2} \int_0^L d\ell_1 \int_0^L d\ell_2 \exp\left[-\frac{\sqrt{(\ell_2 - \ell_1)^2 + (v\tau)^2}}{\ell_o}\right]$$

$$= \frac{8\pi^2 10^{-12}\langle \Delta N^2\rangle}{\lambda^2} \int_0^L dx(L - x) \exp\left[-\frac{\sqrt{x^2 + (v\tau)^2}}{\ell_o}\right]. \tag{4.3}$$

The change of variable $y^2 = 1 + \frac{x^2}{(v\tau)^2}$ gives:

$$\langle a(t)a(t+\tau)\rangle = \frac{8\pi^2 10^{-12}\langle \Delta N^2\rangle \ell_o^2}{\lambda^2} \left\{ \left(\frac{v|\tau|L}{\ell_o^2}\right) \int_1^{\sqrt{1+L^2/(v\tau)^2}} dy \frac{y}{\sqrt{y^2 - 1}} \right.$$

$$\left. \cdot \exp\left[-\frac{v|\tau|y}{\ell_o}\right] - \left(\frac{v|\tau|}{\ell_o}\right)^2 \int_1^{\sqrt{1+L^2/(v\tau)^2}} dy\, y \exp\left[-\frac{v|\tau|y}{\ell_o}\right] \right\} \quad .$$

(4.4)

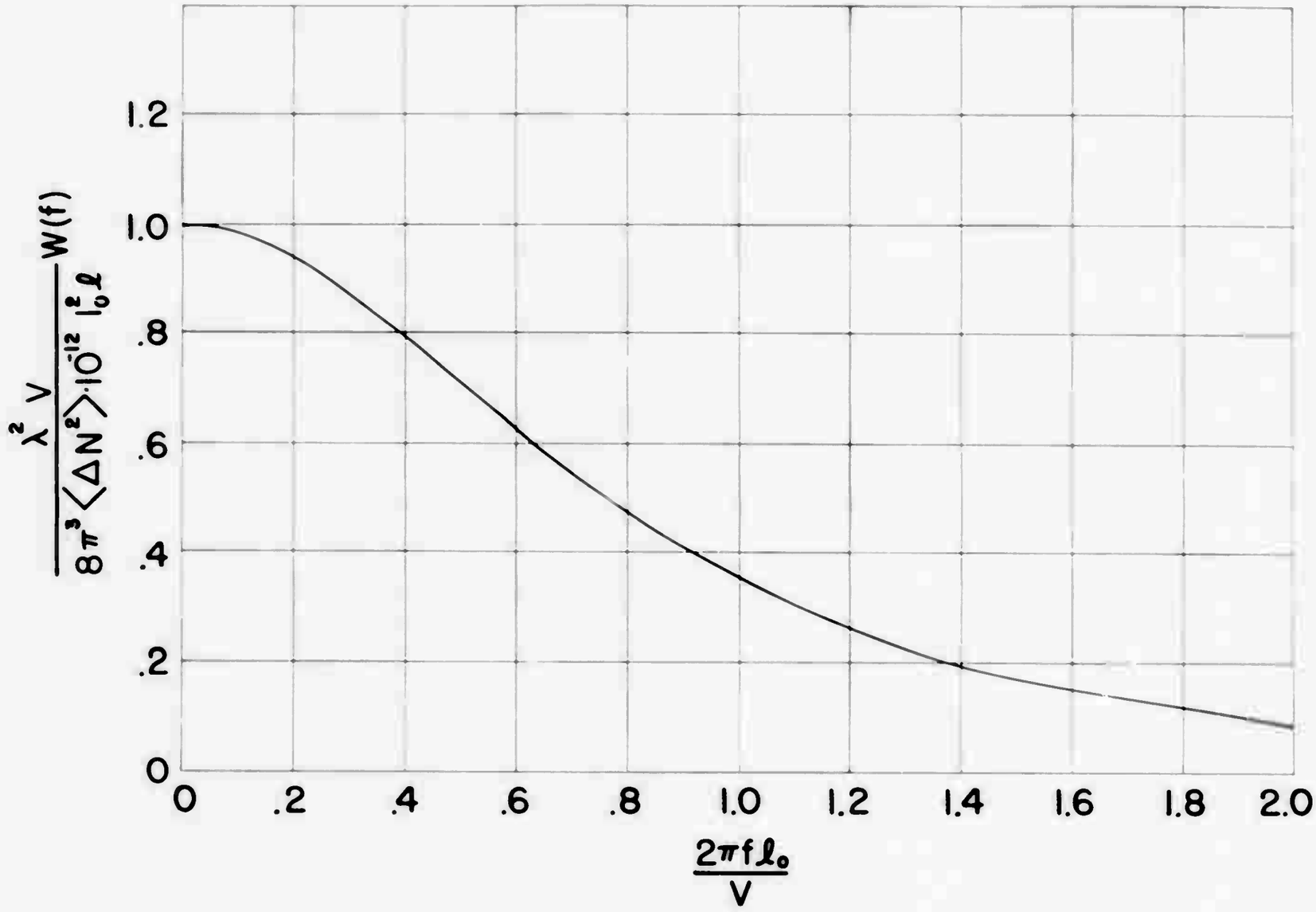

Figure 20

Power Spectrum of Phase for Moving Line-of-Sight

If $L/\ell_o \gg 1$, the upper limit may be relaxed to infinity with small error and the second term neglected in comparison with the first. The integration may then be performed analytically.

$$\langle a(t)a(t+\tau)\rangle \cong \frac{8\pi^2 10^{-12}\langle \Delta N^2\rangle \ell_o^2}{\lambda^2}\left(\frac{v|\tau|L}{\ell_o^2}\right) K_1\left(\frac{v|\tau|}{\ell_o}\right), \qquad (4.5)$$

where K_1 is the modified Bessel function of the second kind. One may verify that this expression reduces to Eq. (2.19) when $\tau = 0$. The cosine transform of Eq. (4.5) yields the power spectrum

$$W(f) = \frac{8\pi^2 10^{-12}\langle \Delta N^2\rangle \ell_o^2}{\lambda^2}\left(\frac{L}{v}\right)\frac{\pi}{\left(1+\frac{4\pi^2 f^2 \ell_o^2}{v^2}\right)^{3/2}}, \qquad (4.6)$$

which is plotted in Figure 20.

(2) Angular Deviations

A ray passing through a turbulent cloud is perturbed in two ways in that it; (1) is bent on entering and again on leaving, and (2) suffers a random deviation of its direction of propagation due to the cumulative effect of the turbulence within the cloud. These two effects will cause the apparent source seen through the cloud to wander about; much as a source of (visual) light viewed through an inhomogeneous window pane apparently changes position as the line of sight traverses it.

Figure 21 pictures an idealized sharp boundary for a typical cloud. The angle of incidence θ_i and refraction θ_o are measured with respect to the cloud's local normal to the boundary. Snell's law relates these angles.

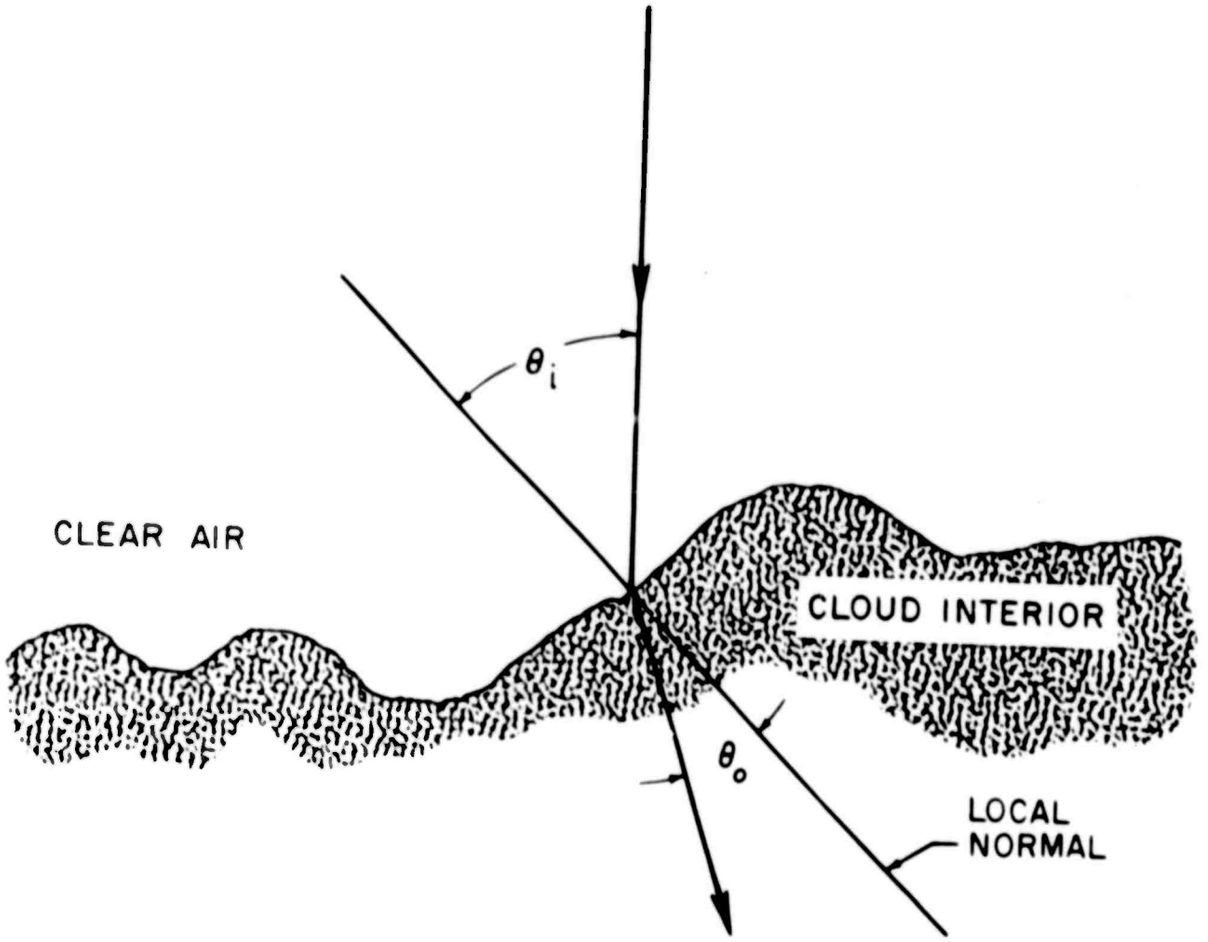

Figure 21

Geometry at Cloud Boundary

$$n_i \sin\theta_i = n_o \sin\theta_o \ . \tag{4.7}$$

Since the effect of diffuse boundaries is quite small, one may put

$$\theta_o = \theta_i - \psi \tag{4.8}$$

where ψ is the (small) deviation produced at the boundary, and

$$n_o' = n_i + \Delta N\, 10^{-6} \tag{4.9}$$

Since $\Delta N \simeq 10$, we may expand Eq. (4.7) to the first order in ΔN and ψ.

$$\psi = \Delta N\, 10^{-6} \tan\theta_i \cong \Delta N\, 10^{-6}\, \theta_i \ . \tag{4.10}$$

Here we have recognized that n_i is very nearly unity. If we assume that the cloud moves through the (stationary) line-of-sight with velocity v, the auto-correlation function for ψ is

$$\langle \psi(t)\,\psi(t+\tau)\rangle = \langle \Delta N(t)\,\Delta N(t+\tau)\rangle\, 10^{-12} \langle \theta_i(t)\theta_i(t+\tau)\rangle \ , \tag{4.11}$$

$$= \langle N^2\rangle 10^{-12} \rho(v\tau) \langle \theta_i^2\rangle R(v\tau) \ , \tag{2.12}$$

where $\rho(r)$ is given by Eq. (2.2) and $R(r)$ is the normalized autocorrelation of the angle of incidence θ_i.

We know very little about the detailed appearance of cloud boundaries (i.e., θ_i) so that we assume for convenience that $R(r) = \rho(r)$. We shall show later that this choice has little significance in considering the total deflection caused by the cloud since the interior dominates over the boundaries. The spectrum for ψ due to the fluctuating boundary is thus:

$$W(f) = \frac{10^{-12} \langle \Delta N^2 \rangle \ell_o}{v} \frac{1}{\left(1 + \dfrac{\pi^2 \ell_o^2 f^2}{v^2}\right)^2} \ . \tag{4.13}$$

The deviation produced by turbulence within the cloud must be added to Eq. (4.13). We choose the situation shown in Figure 19 and the rectangular coordinates oriented with the z-axis along the initial line-of-sight and the x-axis along the direction of cloud motion. The ray deviations are:

$$\phi_x = \int_o^L dz \, \frac{\partial N_1}{\partial x} , \tag{4.14}$$

and

$$\phi_y = \int_o^L dz \, \frac{\partial N_1}{\partial y} ; \tag{4.15}$$

so that the corresponding autocorrelations become

$$\langle \phi_x(t)\phi_x(t+\tau) \rangle = \int_o^L dz_1 \int_o^L dz_2 \left\langle \left. \frac{\partial N_1}{\partial x} \right|_1 \left. \frac{\partial N_1}{\partial x} \right|_2 \right\rangle , \tag{4.16}$$

and

$$\langle \phi_y(t)\phi_y(t+\tau) \rangle = \int_o^L dz_1 \int_o^L dz_2 \left\langle \left. \frac{\partial N_1}{\partial y} \right|_1 \left. \frac{\partial N_1}{\partial y} \right|_2 \right\rangle . \tag{4.17}$$

Using Eq. (2.42) and the rectangular representation for the interval r_{12},

$$r_{12} = \sqrt{(x_2 - x_1)^2 + (y_2 - y_1)^2 + (z_2 - z_1)^2} , \tag{4.18}$$

one can average the gradients in Eq. (4.16) and Eq. (4.17) as,

$$\left\langle \left. \frac{\partial N_1}{\partial u} \right|_1 \left. \frac{\partial N_1}{\partial u} \right|_2 \right\rangle = -\langle N_1^2 \rangle \left[\frac{\xi^2}{r_{12}} \left(\frac{d^2\rho}{dr_{12}^2} - \frac{1}{r_{12}} \frac{d\rho}{dr_{12}} \right) + \frac{1}{r_{12}} \frac{d\rho}{dr_{12}} \right] , \tag{4.19}$$

where u = x or y, and $\xi = x_2 - x_1$ or $y_2 - y_1$ respectively. We shall actually compute Eq. (4.19) for $x_2 - x_1 = v\tau$, $y_2 = y_1 = 0$, and with expression (2.2) for $\rho(r)$.

$$\langle \phi_x(t)\phi_x(t+\tau) \rangle = - \frac{\langle N_1^2 \rangle}{\ell_o} \int_o^L dz_1 \int_o^L dz_2 \left\{ \frac{(v\tau)^2}{(v\tau)^2 + (z_2 - z_1)^2} \right.$$

$$\cdot \left[\frac{1}{\ell_o} \exp\left(- \frac{1}{\ell_o} \sqrt{(v\tau)^2 + (z_2 - z_1)^2} \right) \right.$$

$$\left. + \frac{\exp\left(- \frac{1}{\ell_o} \sqrt{(v\tau)^2 + (z_2 - z_1)^2} \right)}{\sqrt{(v\tau)^2 + (z_2 - z_1)^2}} \right]$$

$$\left. - \frac{\exp\left(- \frac{1}{\ell_o} \sqrt{(v\tau)^2 + (z_2 - z_1)^2} \right)}{\sqrt{(v\tau)^2 + (z_2 - z_1)^2}} \right\}. \qquad (4.20)$$

The integration techniques of Section II B may be applied here to yield:

$$\langle \phi_x(t)\phi_x(t+\tau) \rangle = 2 \cdot 10^{-12} \frac{\langle \Delta N^2 \rangle L}{\ell_o} \left[K_o\left(\frac{v|\tau|}{\ell_o} \right) - \frac{v|\tau|}{\ell_o} K_1\left(\frac{v|\tau|}{\ell_o} \right) \right] . \qquad (4.21)$$

The cosine transform of this expression gives the spectrum as:

$$W(f) = \frac{2\pi 10^{-12} \langle \Delta N^2 \rangle L}{v} \frac{\left(\frac{4\pi^2 \ell_o^2 f^2}{v^2} \right)}{\left(1 + \frac{4\pi^2 \ell_o^2 f^2}{v^2} \right)^{3/2}} \qquad (4.22)$$

which is plotted in Figure 22.

Using the same procedures, one obtains from Eq. (4.17)

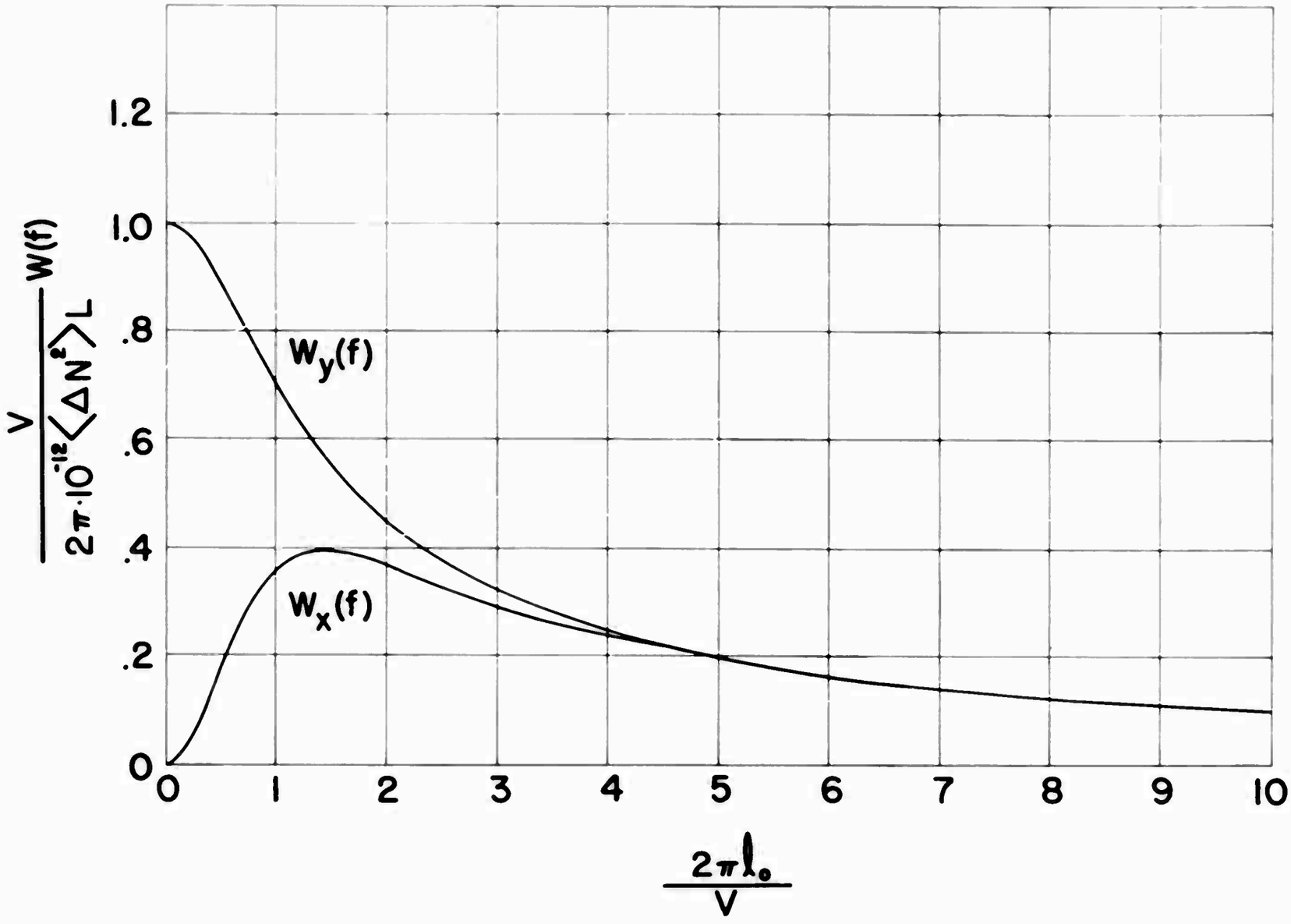

Figure 22

Angle of Arrival Spectra for Moving Line-of-Sight

$$\langle \phi_y(t)\phi_y(t+\tau) \rangle = \frac{2 \cdot 10^{-12} \langle \Delta N^2 \rangle L}{\ell_o} K_o \left(\frac{v|\tau|}{\ell_o} \right) , \tag{4.23}$$

the spectrum of which is also plotted in Figure 22.

$$W(f) = \frac{2\pi 10^{-12} \langle \Delta N^2 \rangle L}{v} \frac{1}{\left(1 + \frac{4\pi^2 \ell_o^2 f^2}{v^2} \right)^{1/2}} \tag{4.24}$$

The remarks made in Part II B concerning the divergence of integrals over these spectra apply here also.

Note that the coefficients of Equations(4.13), (4.22), and (4.24) all contain factors which are of the same order of magnitude except that Eq. (4.13) involves ℓ_o while the others have the factor L. We have consistently assumed that $L \gg \ell_o$ so that it is primarily the interior of the cloud and not the refraction at the boundaries which contributes to the deflection of the ray.

C. Numerical Estimates

Cloud parameters are conspicuous by their absence in the experimental literature. To illustrate the foregoing results however we shall assume ℓ_o = 20 feet, L = 5000 feet, λ = 0.2 feet, and $\left[\langle \Delta N^2 \rangle \right]^{1/2} = 10$. The mean square phase deviation due to scattering is obtained from Figure 4, with $\beta = 4^o$.

$$\langle a_{sc}^2 \rangle = 10^{-3} \text{ rad}^2 . \tag{4.25}$$

The corresponding direct wave result from Eq. (2.19) is:

$$\langle a_{direct}^2 \rangle = 10^{-2} \text{ rad}^2 . \tag{4.26}$$

Clouds thus constitute an important source of phase deviation for any propagation process.

Half power bandwidths for the spectra can be calculated as before. Two different physical situations present themselves. One can imagine the line-of-sight moving through a cloud because of the tracking of a fast moving target. In this case a velocity of 500 fps is quite reasonable. With the above assumptions this yields a bandwidth of about 3 cps. On the other hand, if we consider a stationary line-of-sight with a cloud drifting through at v = 20 fps, one obtains a bandwidth of about 0.12 cps. The preceding estimates apply to phase deviations only. Bandwidths for the angular deviation will be comparable.